New Evaluation and Validation Towards Neutron Reaction Data on Chromium Isotopes at Incident Energies Below 200 MeV*

Wen-Ye Wang (汪文烨) Yin-Lu Han (韩银录) Ji-Min Wang (王记民)† Huan-Yu Zhang (张环宇)‡
Yuan Tian (田源) Xi Tao (陶曦) Hai-Cheng Wu (吴海成) Yong-Li Jin (金永利) Bo-Yu Tan (谭博宇)
Yue Zhang (张玥) Zhao-Hui Wang (王朝辉) Zhi-Gang Ge (葛智刚) Rui-Rui Xu (续瑞瑞)§

China Nuclear Data Center, China Institute of Atomic Energy, Beijing, 102413, China

Abstract: Chromium (Cr) serves as an indispensable structural material in accelerator-driven systems (ADS) and Generation IV reactors, where the precision of its neutron reaction data is important for ensuring reactor safety and operational reliability. However, significant discrepancies persist in both experimental data and evaluations for key reaction channels, such as (n,p) and $(n,2n)$, across the chromium isotopes ^{50,52,53,54}Cr. This study presents a novel evaluation and validation of neutron reaction data for these isotopes at incident energies below 200 MeV, incorporating 571 experimental datasets from EXFOR covering cross sections, angular distributions, energy spectra, and double - differential cross sections. The newly evaluated data provide more reliable key cross sections: the ^{52}Cr$(n,2n)$ cross section resolves discrepancies and supports H.,Liskien et al.'s data; the ^{52}Cr(n,p) cross section aligns well with natural chromium data across all energies, and is validated by competition analysis. The results accurately replicate double differential cross sections and energy spectra, with neutron emission spectra matching experimental peaks and charged - particle spectra agreeing with measurements for ^{50,52}Cr. Moreover, the abundance - weighted sum of (n,p) and $(n,2n)$ cross sections for chromium isotopes agrees well with natural chromium data, confirming systematic consistency. All evaluations are validated using 62 ICSBEP 2014 benchmark facilities with $k_{\rm eff}$ sensitivity to chromium neutron data > 1%. For the PMI002_01 experiment, calculated $k_{\rm eff}$ decreased by ~ 1000 pcm relative to CENDL - 3.2, improving agreement with the benchmark; in the OKTAVIAN shielding benchmark, the neutron leakage spectrum also produces experiments well.

Keywords: Neutron-induced reaction, cross sections, energy spectra, angular distributions, nuclear model theory.

DOI: **CSTR:**

I. INTRODUCTION

Chromium (Cr), essential in stainless steel, is key for Accident Tolerant Fuel (ATF) coatings[1, 2], structural materials in Gen IV reactors[3, 4], and Accelerator-Driven System (ADS)[5],attracting broad interests in the nuclear data research. Natural Cr consists of four isotopes, namely ^{50}Cr (4.345%), ^{52}Cr (83.789%), ^{53}Cr (9.501%), and ^{54}Cr (2.365%). Extensive nuclear data evaluations for these isotopes have been performed as listed in Table 1. The evaluations of n+ ^{50,52,53,54}Cr reactions are included in the major evaluation libraries, and the nuclear reaction cross sections for important channels (n,el), (n,inl), (n,γ), (n,p), $(n,2n)$, angular distributions and double differential cross sections for particle emission are provided. In addition, in the recent study of International Nuclear Data Evaluation Network (INDEN) in IAEA, the neutron data of ^{52}Cr in good quality are also presented.

Significant discrepancies still exist between the evaluated data and measurements. Taking the ^{52}Cr(n,p) reaction cross sections as an example, significant discrepancies can be observed above neutron energy 14 MeV, as shown in Fig. 1. At the same time, as for the ^{52}Cr$(n,2n)$

Received 15 January 2026

* Supported by the following grants: the Nuclear Technology Research and Development Project of State Administration of science,Tecnology and Industry for National Defence of China (No. HJSYF2024(01)), the National Key Research and Development Program of the Ministry of Science and Technology (No. 2022YFA1602403), the "Ye Qisun" Science Fund of the National Natural Science Foundation of China (No. U2541242), the Key Program of the National Natural Science Foundation of China (No. KZ77088701), and the Young Scientists Fund of the National Natural Science Foundation of China (No. 12005303), the Science Fund of the National Natural Science Foundation of China (No. U2441221)

† E-mail: jmwang@ciae.ac.cn
‡ E-mail: zhanghuanyu@ciae.ac.cn
§ E-mail: xuruirui@ciae.ac.cn

Table 1. The evaluation status of n+ ^{50,52,53,54}Cr in major libraries.

Major Libraries	Place	Year	First Author	Energy	Information of evaluation	Ref.
INDEN-Aug2023	IAEA	2020	G. Nobre	200 MeV	New evaluation from BNL, ORNL, IAEA	[6]
ENDF/B-VIII.1	USA	2024	G. Nobre	65 MeV	Taken from INDEN-Aug2023	[7]
JEFF-4.0	Europe	2025	G. Nobre	65 MeV	Taken from ENDF/B-VIII.1	[8]
JENDL-5	Japan	2021	N. Iwamoto	200 MeV	Evaluated in 2009 and revised in 2021 by N. Iwamoto	[9]
CENDL-3.2	China	2020	B.S. YU	20 MeV	Evaluated by Bao-Sheng YU in 1991; Revised by Haicheng WU in 2009	[10]
BROND-3.1	Russia	2016	V. G. Pronyaev	20 MeV (For ^{50}Cr 150 MeV)	^{50,54}Cr: Taken from ENDF/B-VII.1 (S. Chiba); ^{52}Cr: 1995 by V.G. Pronyaev; ^{53}Cr: Mainly from JENDL-3.0 (S. Chiba, 1997)	[11]
TENDL-2023	IAEA	2023	A.J. Koning	200 MeV	Evaluated by TALYS	[12]

Note: All abbreviations are defined in Appendix A.

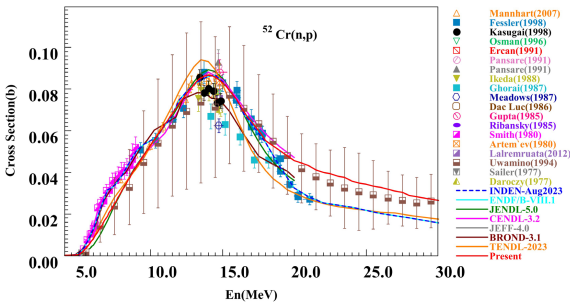

Fig. 1. (color online) Experimental and evaluated data of protect ^{52}Cr(n,p) cross sections.

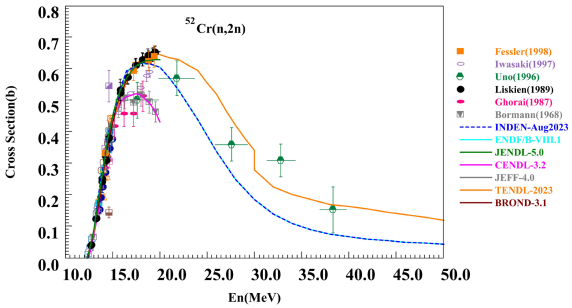

Fig. 2. (color online) Experimental and evaluated data of protect ^{52}Cr$(n,2n)$ cross sections.

reaction, the experimental data for the neutron energy surpass 15 MeV exhibit substantial discrepancies up to 200 mb, as illustrated in Fig. 2, which deduce the big difference for various libraries. Therefore, more elaborate study to understand these differences are required.

To address these issues, we perform a new evaluation and analysis for neutron data of n+ ^{50,52,53,54}Cr nuclear reaction systems at neutron energies below 200 MeV. Following the approach outlined in Ref. [13−15], we conduct experimental data evaluation by focusing on 571 datasets covering cross sections, angular distributions, energy spectra, and double differential cross sections. To ensure a rigorous evaluation of the measured data quality, a full consideration is given to various factors, including experimental methods, neutron source properties, samples, detection techniques, and other relevant technical aspects. Consequently, based on this systematic and in - depth assessment, it is highly recommended to employ a complete experimental dataset to provide solid support for the current evaluation.

Regarding the theoretical calculation study, the principal nuclear reaction processes under consideration are illustrated in Fig. 3. As the incident neutron energy increases, a broader range of nuclear reaction mechanisms gradually come into play, with the dominant reaction mode transitioning from statistical equilibrium emission to pre - equilibrium and direct reaction pathways.

In our research, we first utilize the Chinese nuclear reaction code UNF[16] to handle neutron data within the energy range spanning from a few keV to 20 MeV. This code is well suited for capturing the relevant nuclear reaction characteristics in this relatively lower energy regime. Subsequently, to extend our calculations to a higher energy range, we employ another Chinese nuclear reaction code, MEND[17]. This code enables us to compute the complete set of nuclear reaction data for energies below 200 MeV. By integrating the results from these two codes, we have successfully accomplished new evaluations of neutron data for the chromium isotopes ^{50}Cr, ^{52}Cr, ^{53}Cr, and ^{54}Cr. Moreover, our study offers in - depth analysis regarding the discrepancies in reactions such as (n,p) and $(n,2n)$, providing valuable insights into the underlying nuclear reaction mechanisms.

The paper is arranged as follows. The details of experimental data evaluation are introduced in Sec. II; Section III briefly outlined the current theoretical models; Section IV make comparison and analysis for the evaluated results; An integral examination for ^{52}Cr are exampled in Section V; Finally, a brief summary is presented in Section VI.

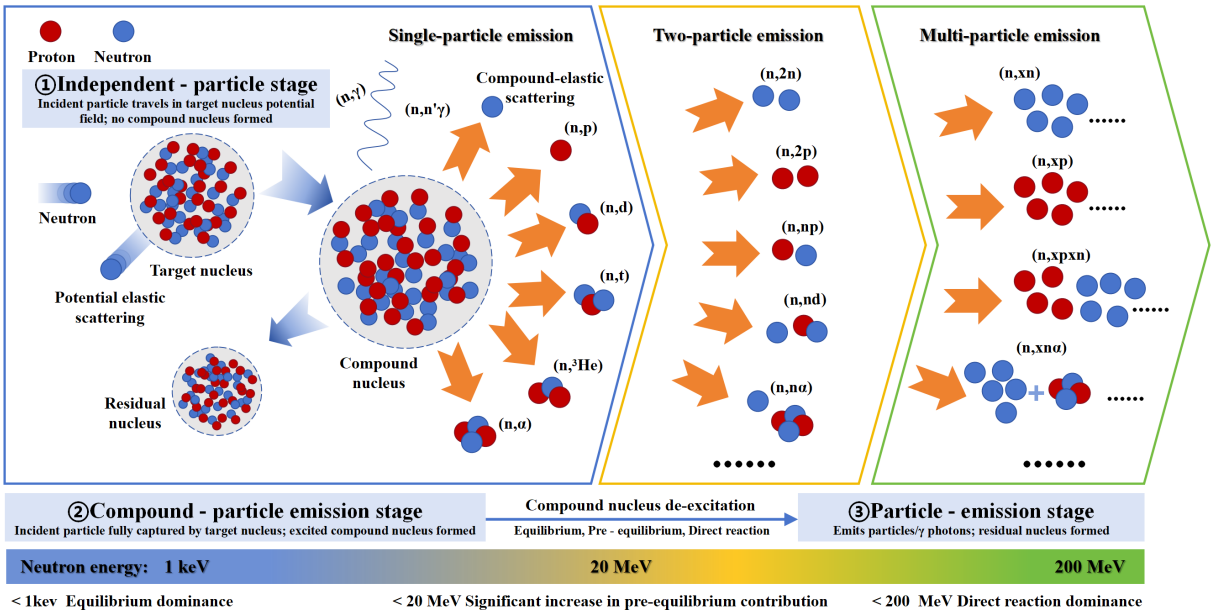

Fig. 3. (color online) Neutron reaction scheme for Cr isotopes with neutron energy below 200 MeV.

II. EXPERIMENTAL DATA ANALYSIS

Based on Experimental Nuclear Reaction Data (EXFOR)[18] database, we investigate 571 sets of experimental data from different measurements reported for n+ ^{50,52,53,54,nat}Cr systems. These data are diverse in type, covering cross sections, angular distributions, energy spectra, and double differential cross sections. The majority of the 547 measurement sets provide values below 20 MeV, with only 24 sets recorded at energies from above this threshold up to 200 MeV. Although the measurements in higher energy region are limited, they are also highly concentrated in our work to satisfy the evaluated results within 200 MeV, which are presented in Table 2, and all types are cross sections.

In this table, it is observed that for natural chromium and ^{52}Cr, abundant experimental data exist for the total cross section, elastic scattering cross section, and elastic angular distributions. The total cross section data extend up to 80.62 MeV, enabling the extraction of reliable phenomenological optical-model parameters in the high energy region. Based on the systematic A and Z dependence of the phenomenological optical model, these parameters are extrapolated to describe the chromium isotopes ^{50}Cr, ^{53}Cr, and ^{54}Cr. In energy regions where experimental data are scarce, the results rely on theoretical models to ensure physical consistency. In the 20-200 MeV range, hundreds of nuclear reaction channels open, leading to strong competition among multiple pathways. As a result, direct measurement of individual reaction channel cross sections becomes challenging. Therefore, above 20 MeV, experimental data on emission energy spectra or double differential cross sections for particles including n, p, d, t, ^{3}He, and α are urgently needed to fill the measurements gap. Such data are vital for validating and refining theoretical models.

With respect to the data below 20 MeV, the measurements for major nuclear reactions $(n,tot),(n,el),(n,inl),(n,\gamma),(n,p),(n,d),(n,\alpha),(n,2n)$ et al. in Fig. 3 are all considered. To thoroughly evaluate the measured data, the experimental methods like activation, time-of-flight are systematically analyzed based on the original literature. Neutron sources (like type, neutron flux, monochromaticity), sample properties (like physical properties of samples, composition, purity, shape, and surface finish et al.), detection techniques (like detector type, resolution, and background) are over viewed. By integrating these considerations with rigorous experimental design and data validation, we establish experimental datasets by evaluating data reliability to support our assessment. The original experimental data and literature reports serve as the most important basis for investigation. We conducted a physical evaluation of the experimental data, which is primarily based on key factors of the experiments (experimental method, neutron source, detector, sample quantification, monitor, and decay data). Additional considerations included the year, laboratory, publication channel, and institution. Furthermore, the influence of nuclear reaction mechanisms is taken into account. A weight assignment and evaluation are performed on all experimental data to enhance reliability, with specific datasets being highlighted to support our assessment. Given the extensive volume of experimental data, this paper only provides briefly tabulated experimental lists in Appendix C, details can also be consulted in the EXFOR database.

Here, using the evaluation oaref ^{52}Cr$(n,2n)$ cross sections as an illustrative instance, we analyze 21 sets of ex-

Table 2. Information on experimental data at energies above 20 MeV

Year	Author	Reaction	Source	Method	Detector	En(MeV)	Points	EXFOR Entry
1980	S. M. Qaim	$^{50}Cr(n,3n)^{48}Cr$	D-BE	ACTIV, CHSEP	GELI, SILI	20.0-30.0	1	21649
1992	Y. Uwamino	$^{50}Cr(n,3n)^{48}Cr$	P-BE	ACTIV	GE-IN	26.5-38.5	13	22703
1978	S. M. Qaim	$^{50}Cr(n,x)^{48}V$	D-BE	ACTIV, CHSEP	GELI	22.5	1	20840
2007	V. Semkova	$^{50}Cr(n,x)^{48}V$	D-T	ACTIV, GSPEC	HPGE, LONGC	17.3-20.6	5	22877
2000	R. F. Carlton	$^{52}Cr(n,tot)$	-	TOF, TRN	SCIN	0.050-69.13	25833	13840
1990	N. Olsson	$^{52}Cr(n,n')$	D-T	TOF	SCIN	21.6	1	22128
1998	A. Fessler	$^{52}Cr(n,p)^{52}V$	D-T, D-D	ACTIV, TOF, GSPEC	HPGE, BF3, SCIN	9.31-21.07	22	22406
1996	Y. Uno	$^{52}Cr(n,2n)^{51}Cr$	P-^{7}Li	ACTIV, TOF	GE-IN	17.6-38.3	5	22702
1980	S. M. Qaim	$^{53}Cr(n,3n)^{51}Cr$ $^{53}Cr(n,^{3}He)^{51}Ti$	D-BE	ACTIV, CHSEP	GELI, SILI	20.0-30.0	2	21649
1998	A. Fessler	$^{53}Cr(n,p)^{53}V$ $^{53}Cr(n,x)^{52}V$	D-T, D-D	ACTIV, TOF, GSPEC	HPGE, BF3, SCIN	11.57-21.07	24	22406
1998	A. Fessler	$^{54}Cr(n,\alpha)^{51}Ti$ $^{54}Cr(n,p)^{54}V$ $^{54}Cr(n,x)^{53}V$	D-T, D-D	ACTIV, TOF, GSPEC	HPGE, BF3, SCIN	16.02-20.24	15	22406
2001	W. P. Abfalterer	$^{nat}Cr(n,tot)$	EVAP	TOF	SCIN	5.29-559.1	467	13753
1980	D. C. Larson	$^{nat}Cr(n,tot)$	PHOTO	TOF	SCIN	2.00-80.62	685	12882
1973	F. G. Perey	$^{nat}Cr(n,tot)$	-	-	-	0.19-29.50	3658	10342
1968	S. Cierjacks	$^{nat}Cr(n,tot)$	EVAP	TOF, TRN	SCIN	4.41-31.94	1231	20012
1960	J. M. Peterson	$^{nat}Cr(n,tot)$	D-T	-	SCIN	17.5-28.6	4	11108
1987	N. Olsson	$^{nat}Cr(n,el)$	D-T	TOF	SCIN; SCIN	21.6	1	22048
1977	G. F. Auchampaugh	$^{nat}Cr(n,2n)$	D-T; D-T	-	STANK; STANK; SCIN	14.7-21.0	7	12936
1994	Y. Uwamino	$^{nat}Cr(n,x)^{52}V$	P-BE	ACTIV	GE-IN	5.5-38.5	34	22700
1994	Y. Uwamino	$^{nat}Cr(n,x)^{53}V$	P-BE	ACTIV	GE-IN	4.5-38.5	35	22700

Note: All abbreviations are defined in Appendix A.

perimental data. As shown Fig. 4, 14 sets are populated for neutron energy below 15 MeV using D-T neutron source and activation methods, and the reported values are in good agreement with each other across this energy region; however, for energy above 15 MeV, obvious discrepancies are exhibited even up to 200 mb in the rest six sets (EXFOR Entry: 22406, 22755, 22702, 22124, 12958, 20834). All six sets are performed using the activation method[19]. In contrast to the data by Bormann (1968) and Ghorai (1987), the remaining four sets of newly measured data are generally 200 mb higher around 20 MeV. These new measurements use HpGe detectors, which not only fixe the problems of NaI detectors (low energy resolution and easy to absorb moisture) but also solve the issues with Ge(Li) detectors, like needing constant low - temperature cooling, having complex production steps, small sensitive areas, and being easily damaged by radiation. Moreover, isotopic samples of ^{52}Cr with a purity of 99.9% are utilized, effectively reducing interference from competing reaction channels of other isotopes (e.g., $^{50}Cr(n,\gamma)$ and $^{54}Cr(n,2n)$). It is explicitly stated in Ref. 24 that a systematic underestimation of 20%–30% is exhibited in Ghorai's measurement in 1987.

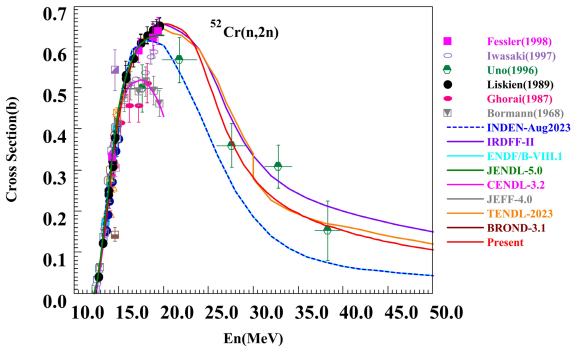

Fig. 4. (color online) Comparison of $^{52}Cr(n,2n)$ cross sections between evaluated data (red curve) and experimental data (symbols).

The latest INDEN-Aug2023 and IRDFF-II[20] evaluations support higher cross-sections values. Therefore, the $^{52}Cr(n,2n)$ cross sections by Liskien and Fessler are adopted in this work. For the energy region above 20 MeV, the measurement data from Uno (1996) is recommended. The solid red line in Fig. 4 is our new evaluated values.

III. THEORETICAL MODELS

Theoretical calculation of nuclear reactions in this work comprises three key stages. Firstly, the independent particle stage, detailing scattering / absorption between incident particles & target nucleus, must be considered across all neutron incident energies. It is described by the optical model potential based on the Woods-Saxon formula, for neutron. Secondly, the composite particle emission stage, which is divided into statistical equilibrium, pre-equilibrium, and direct reaction processes. As the incident neutron energy increases, the dominant reaction mechanism governing particle emission evolves.

In our calculations, when dealing with neutron energies below 20 MeV, we employ a unified approach that combines the Hauser-Feshbach and exciton models, as detailed in Ref. [21]. The UNF code, grounded in this unified model, takes into account both the conservation of angular momentum and recoil effects. It demonstrates a high degree of theoretical self-consistency, making it well suited for high precision data evaluation. To improve agreement with the experimental data, the level density parameter α and the pair correction parameters Δ are optimized according to the measurements, and the final values are listed in Appendix B for each reaction.

For neutron energies below 200 MeV, the MEND code offers broader coverage (up to 250 MeV). It integrates key nuclear reaction models—including the optical, evaporation, cascade emission, exciton, and Hauser-Feshbach (HF) theories—to support multi-particle and multi-stage emission processes. In this work, we systematically optimize its parameters using Su Zongdi's[22] theoretical framework, resulting in an improved parameter set. Given the large number of parameters involved, specific numerical values are omitted here.

MEND and UNF are constructed within the same general reaction-model framework. The main difference lies in the treatment of angular-momentum and parity conservation, which reflects their respective energy domains and design goals.

In the UNF code, an angular-momentum–dependent exciton model combined with a fully J^{π} resolved Hauser–Feshbach formalism is employed, ensuring strict conservation of angular momentum and parity throughout the reaction process. This treatment is essential in the low-energy regime, where individual compound-nuclear states and selection rules play a dominant role.

With increasing incident energy ($E_n \gtrsim 20\,\mathrm{MeV}$), the influence of detailed J^{π} conservation on inclusive observables gradually diminishes due to the increasing number of open channels and the dominance of multi-step, non-equilibrium processes. Accordingly, in MEND the reaction mechanism is organized as follows. Direct reaction contributions (for discrete levels taken as external input, and for continuum states described by empirical systematics) are evaluated first. Fast intranuclear cascade neutron emission is then described using empirical formulae and treated separately from the statistical stages. Pre-equilibrium emission is modeled with the standard exciton model, while the equilibrium decay is treated with a simplified evaporation model obtained as the high-energy limit of the Hauser–Feshbach formalism. In the cascade, pre-equilibrium, and evaporation stages, angular-momentum and parity conservation are not treated explicitly.

This hierarchical mechanism chain allows MEND to provide a consistent description of reaction cross sections and spectra up to ~200 MeV, while keeping the computational complexity under control. A short subsection and a schematic summary have been added to the revised manuscript to make this organization explicit.

In addition, the contribution of direct reaction for inelastic scattering cross sections and angular distributions of discrete levels for n+ ^{50,52,53,54}Cr reactions are determined by the DWUCK4[23] code performing the distorted wave Born approximation. The information on discrete energy levels is obtained from the Reference Input Parameter Library-3 (RIPL-3)[24]. Theoretical calculations consider 7, 8, 15, and 7 discrete levels, which contribute to direct reactions on ^{50,52,53,54}Cr.

IV. RESULTS AND ANALYSIS

Based on the evaluation of experimental data and theoretical model calculations, we have obtained a new set of evaluated results. The detailed discussion and analysis are presented below:

A. Cross sections and angular distributions

1. *Total and elastic cross sections*

For ^{52}Cr and ^{53}Cr, experimental data exhibit significant fluctuating structures in the low-energy region, while our results reasonably reproduce their average values. Based on comprehensive evaluation and analysis, the ENDF/B-VIII.1 evaluated data are recommended for energies below 7 MeV, with resonance parameters adopted from L. C. Leal et al. (2010)[25]. Comparisons between the evaluated data (ENDF/B-VIII.1 and JENDL-5) and experimental data are shown in Fig. 5 and 6. The isotopic abundance of ^{52}Cr is as high as 83.789%. Therefore, our results have also been compared with the experimental data for natural chromium. The data for ^{nat}Cr from Abfalterer (2001) (EXFOR Entry: 13753) and Larson (1980) (EXFOR Entry: 12882) are compared with the result of n+ ^{52}Cr reaction, as shown in Fig. 5.

The experimental data for the n+ ^{50,54}Cr reactions total cross sections are mainly concentrated in the resonance energy region. A. I. Dyumin (EXFOR Entry: 40149)

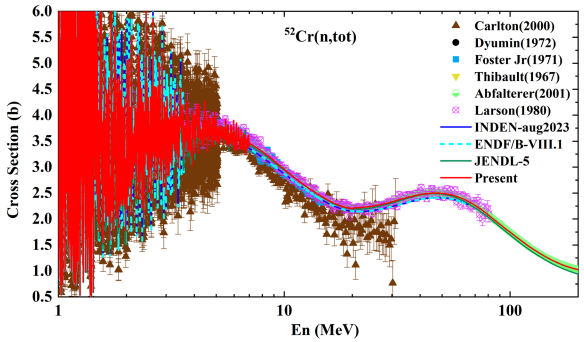

Fig. 5. (color online) Comparison of ^{52}Cr(n,tot) cross sections between evaluated data (red curve) and experimental data (symbols).

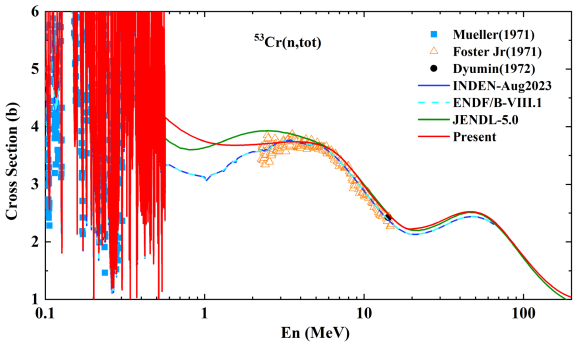

Fig. 6. (color online) Comparison of ^{53}Cr(n,tot) cross sections between evaluated data (red curve) and experimental data (symbols).

have published the experimental data for the n+ ^{50,52,53,54}Cr reactions total cross sections at 14.2 MeV in 1972. The results of the total cross sections for n+ ^{50,52,53,54}Cr reactions show excellent agreement with existing experimental data.

The comparisons of the results with existing experimental data for the elastic scattering cross sections of n+ ^{52}Cr reaction are shown in Fig. 7. The experimental datasets comprises both ^{52}Cr and natural chromium elastic scattering cross sections: the top two sets correspond to ^{52}Cr data, while the latter four represent natural chromium data. Among these, I. A. Korzh et al. (1977) (EXFOR Entry: 40557) have measured elastic cross sections for ^{50,52,54}Cr reactions, and the results show good agreement with these data.

2. *Elastic scattering angular distributions*

Fig. 8 display the comparisons between the evaluated results and the experimental data for the elastic scattering angular distributions. I. A. Korzh et al. (1975) (EXFOR Entry: 40531) have measured the elastic scattering angular distributions of ^{50,52,54}Cr for incident neutron energies from 1.5 to 3.0 MeV, and the theoretical results agree well with the existing experimental data. Fig. 9 shows the

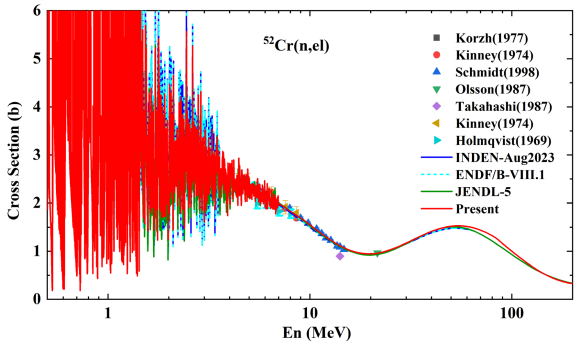

Fig. 7. (color online) Comparison of ^{52}Cr(n,el) cross sections between evaluated data (red curve) and experimental data (symbols).

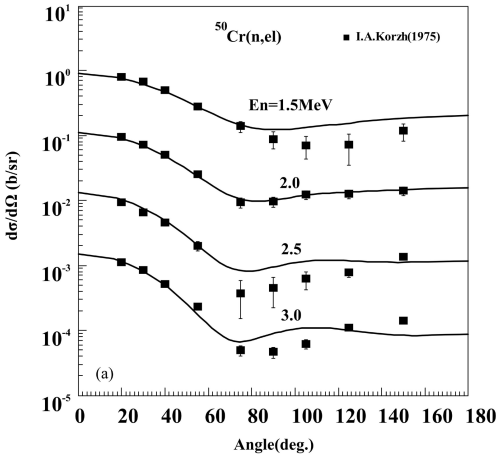

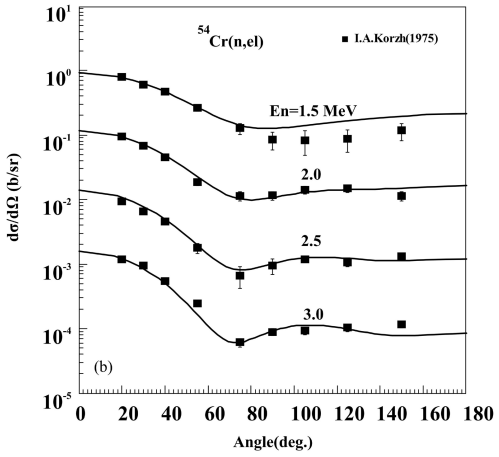

Fig. 8. Comparisons of elastic scattering angular distributions for ^{50,54}Cr(n,el) between evaluated data (solid lines) and experimental data reported by I.A.Korzh (1975) (symbols). The energy region covers from 1.5 MeV to 3.0 MeV. In each panel, the topmost curve for 1.5 MeV remains the true reported values in the literature, and the other results from 1.5 MeV to 3.0MeV are multiplied by factors of 0.1, 0.01, and so on, respectively.

comparison between the elastic scattering angular distributions of n+ ^{50,54}Cr reactions and the experimental data

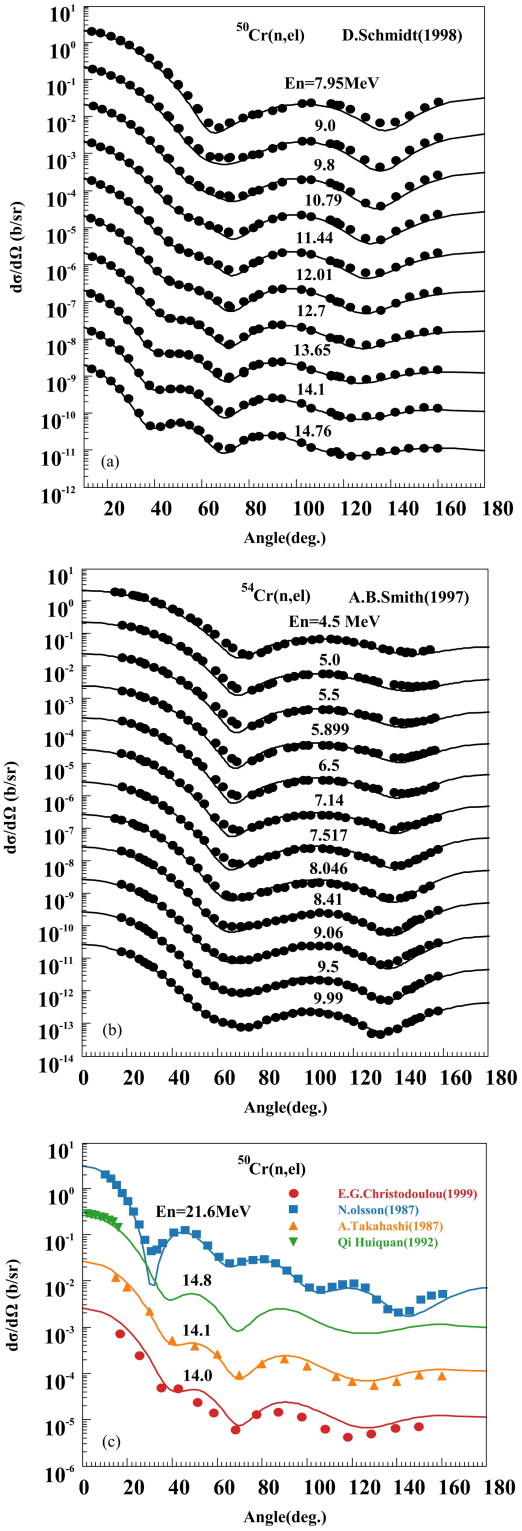

Fig. 9. (color online) Comparisons of elastic scattering angular distributions for ^{50,54}Cr(n,el) between evaluated data (solid lines) and natural chromium experimental data (symbols). In each panel, the topmost curve remains the true reported values in the literature, and the other results from top to bottom are multiplied by factors of 0.1, 0.01, and so on, respectively.

for natural chromium. One can see that the theoretical results agree well with the experimental data.

As shown in Fig. 5-9, the theoretical results exhibit excellent agreement with experimental data across the entire angular range. This demonstrates that the obtained neutron optical model potential parameters give a good description of the measured elastic and inelastic scattering angular distributions.

3. *Inelastic scattering angular distributions*

The inelastic scattering angular distributions for ^{50}Cr(n,n_1) (to the discrete excited level of 0.7833 MeV, 2+) and ^{54}Cr(n,n_1) (to the discrete excited level of 0.8349 MeV, 2+) at incident neutron energies from 1.5 to 3.0 MeV are compared with the experimental data reported by I. A. Korzh et al. (EXFOR Entry: 40531) as shown in Fig. 10.

The inelastic scattering angular distributions for ^{52}Cr(n,n_1) and ^{52}Cr(n,n_2) (to the discrete excited level of 0.7833 MeV, 2+ and 2.3696 MeV, 4+) at incident neut-

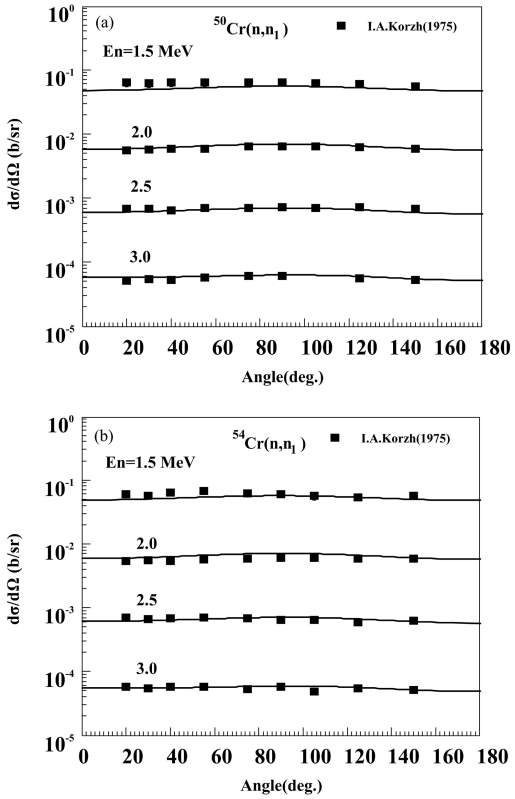

Fig. 10. Comparisons of inelastic scattering angular distributions for ^{50,54}Cr(n,n_1) between evaluated data (solid lines) and experimental data reported by I.A.Korzh (1975) (symbols). The energy region covers from 1.5 MeV to 3.0 MeV. In each panel, the topmost curve for 1.5 MeV remains the true reported values in the literature, and the other results from 1.5 MeV to 3.0 MeV are multiplied by factors of 0.1, 0.01, and so on, respectively.

ron energies from 4.07-8.56 MeV are compared with the natural chromium experimental data reported by W. E. Kinney et al. (EXFOR Entry: 10413) as shown in Fig. 11-13. A comparison of the two angular distributions shows that the inelastic scattering angular distribution for the first discrete level exhibits a pronounced forward-peaking tendency, while that for the second discrete level is approximately isotropic. This reflects the J^{π} dependence inherent in the unified exciton model and Hauser–Feshbach theory at energies below 20 MeV.

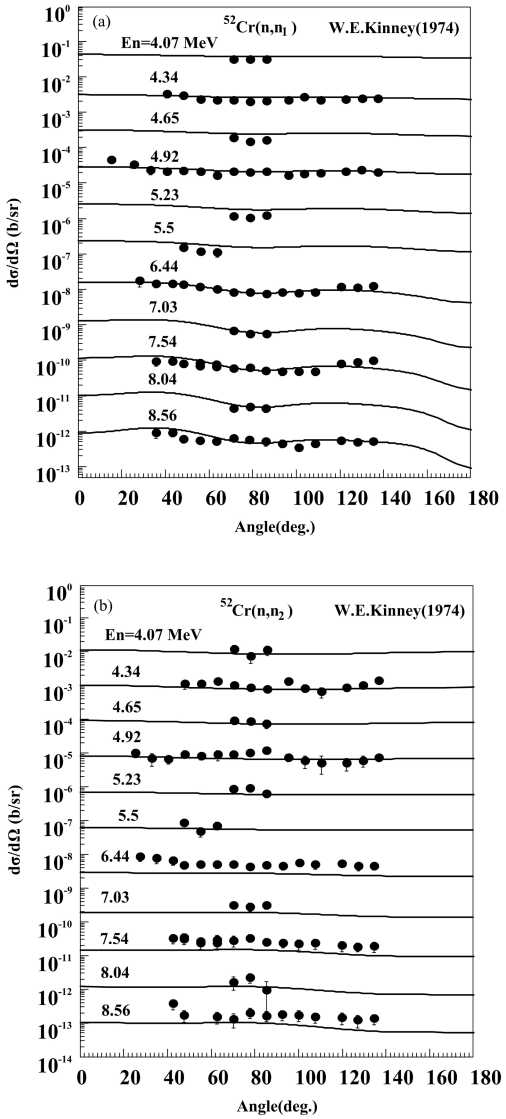

Fig. 11. Comparisons of inelastic scattering angular distributions for ^{52}Cr(n,n_1) and ^{52}Cr(n,n_2) between evaluated data (solid lines) and experimental data of natural Cr reported by W.E.Kinney (1974) (symbols). The energy region covers from 4.07 MeV to 8.56 MeV. In each panel, the topmost curve for 4.07 MeV remains the true reported values in the literature, and the other results from 4.34 MeV to 8.56 MeV are multiplied by factors of 0.1, 0.01, and so on, respectively

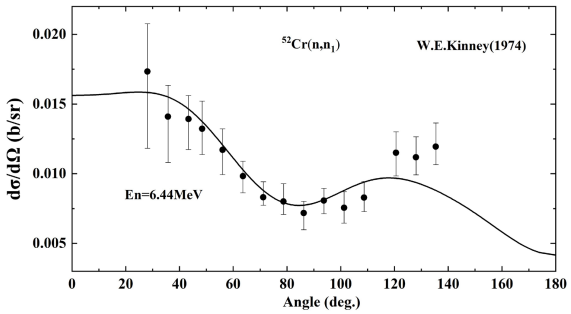

Fig. 12. Comparison of inelastic scattering angular distributions for the first discrete level of ^{52}Cr between evaluated data (solid lines) and natural chromium experimental data reported by W.E.Kinney (1974) (symbols).

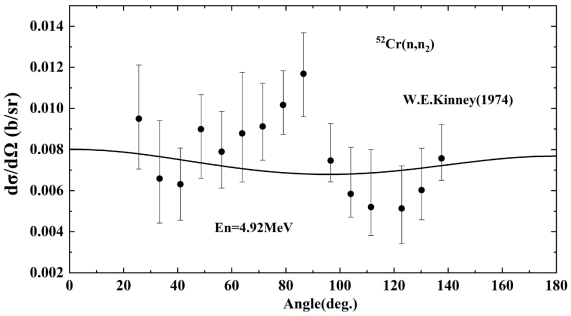

Fig. 13. Comparison of inelastic scattering angular distributions for the second discrete level of ^{52}Cr between evaluated data (solid lines) and natural chromium experimental data reported by W.E.Kinney (1974) (symbols).

4. *Inelastic cross sections*

In nuclear reaction processes, the contributions to inelastic scattering come from direct reactions, pre-equilibrium reactions, and statistical equilibrium reactions. At lower energies, statistical equilibrium reactions play a dominant role. As the energy increases, the contribution of direct reactions to inelastic scattering becomes more and more significant. A comparison between the evaluated results and experimental data for the inelastic scattering cross sections of ^{50,53,54}Cr reactions is shown in Fig. 14. Recently, Tan Boyu et al.[26] from the China Institute of Atomic Energy (CIAE) utilize the HI-13 Tandem Accelerator to generate monoenergetic neutrons with energies of 5.62 MeV, 6.24 MeV, and 7.95 MeV via the $D(d,n)^3He$ reaction. Employing the prompt γ -ray measurement method combined with a CLOVER-type high-purity germanium (HpGe) detector array, they successfully obtain the first experimental measurements of the production cross sections of five characteristic γ -rays of ^{52}Cr in China. Correction terms for γ -ray self-absorption, neutron flux attenuation, and multiple scattering are incorporated during the experiment, resulting in a total uncertainty of only 6.5% for the final measurement results, which indicates superior precision. Notably, our results

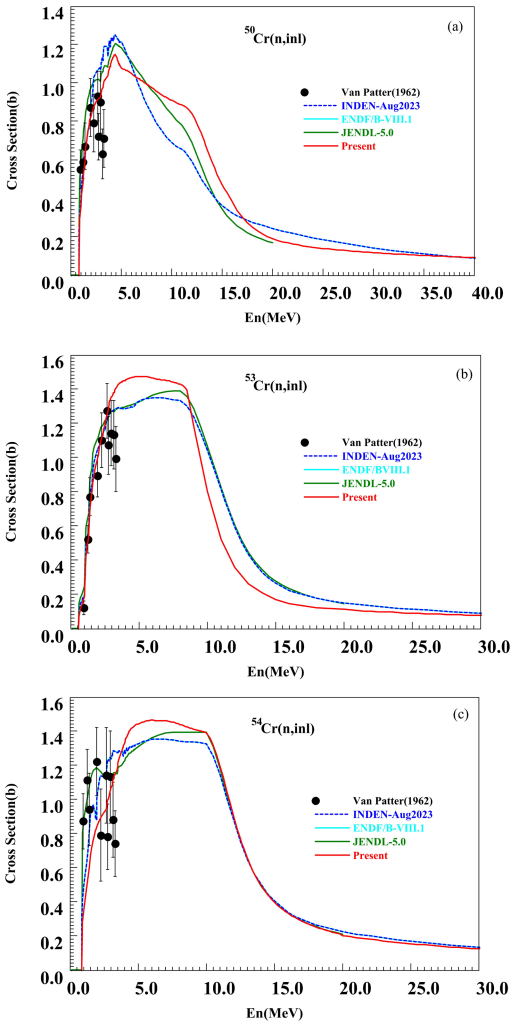

Fig. 14. (color online) Comparison of ^{50,53,54}Cr(n,inl) cross sections between evaluated data (red curve) and experimental data (symbols).

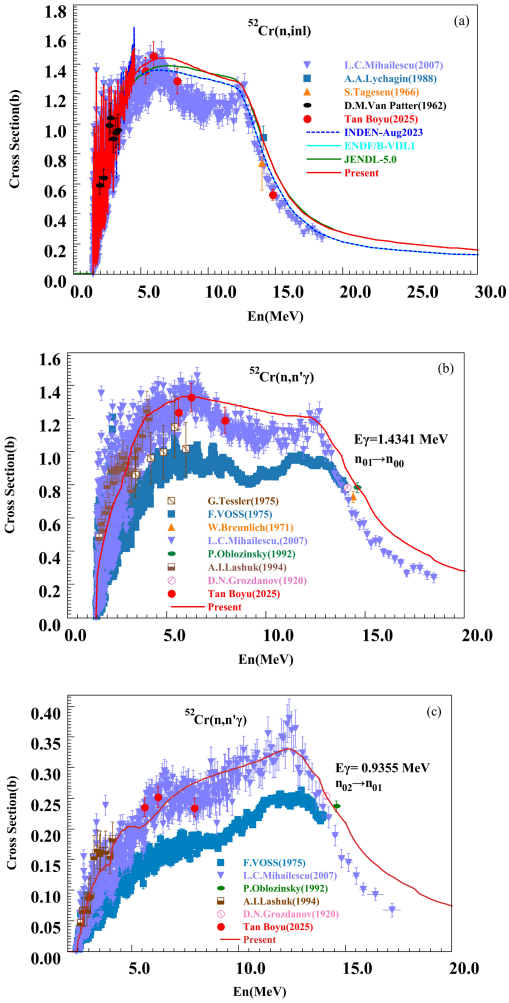

Fig. 15. (color online) Comparison of discrete levels' inelastic cross sections and inelastic scattering gamma production cross sections for ^{52}Cr between evaluated data (red curve) and experimental data (symbols).

can achieve excellent agreement with this high-precision experimental data, which Fig. 15 shows. For the inelastic scattering cross sections of n+ ^{50,52,53,54}Cr reactions the evaluated results agree well with the low energy experimental data measured by D. M. Van Patter et al. (EXFOR Entry: 11676).

Based on experimental data for inelastic scattering cross sections and inelastic scattering gamma production cross sections of discrete levels, the theoretical results for some discrete levels are compared.

Fig. 16(a)(b), Fig. 17(a)(b) and Fig. 18(a)(b), show the comparisons of evaluated results for discrete level inelastic scattering cross sections with existing experimental data. Among these, the inelastic scattering cross sections experimental data for ^{50,54}Cr measured by I. A. Korzh et al. (EXFOR Entry: 40531) are consistent with the results. The experimental inelastic scattering cross sections data for ^{50,52,53}Cr measured by P. T. Karatzas et al. (1978) (EXFOR Entry: 10492) – deduced from inelastic gamma-ray production cross sections scaled by natural isotopic abundances – show good agreement with theoretical results after normalization by isotopic abundances.

Fig. 16(c)(d) show the comparisons of inelastic scattering gamma production cross sections evaluated results with existing experimental data for transitions from the first excited state to the ground state, and from the second excited state to the first excited state. Fig. 17(c)(d) show the comparisons of inelastic scattering gamma production cross sections evaluated results with existing experimental data for transitions from the first excited state to the ground state, and from the third excited state to the ground state. Fig. 18(c)(d) show the comparisons of inelastic scattering gamma production cross sections evaluated results with existing experimental data for transitions from the first excited state to the ground state, and from the third excited state to the first excited state. G.

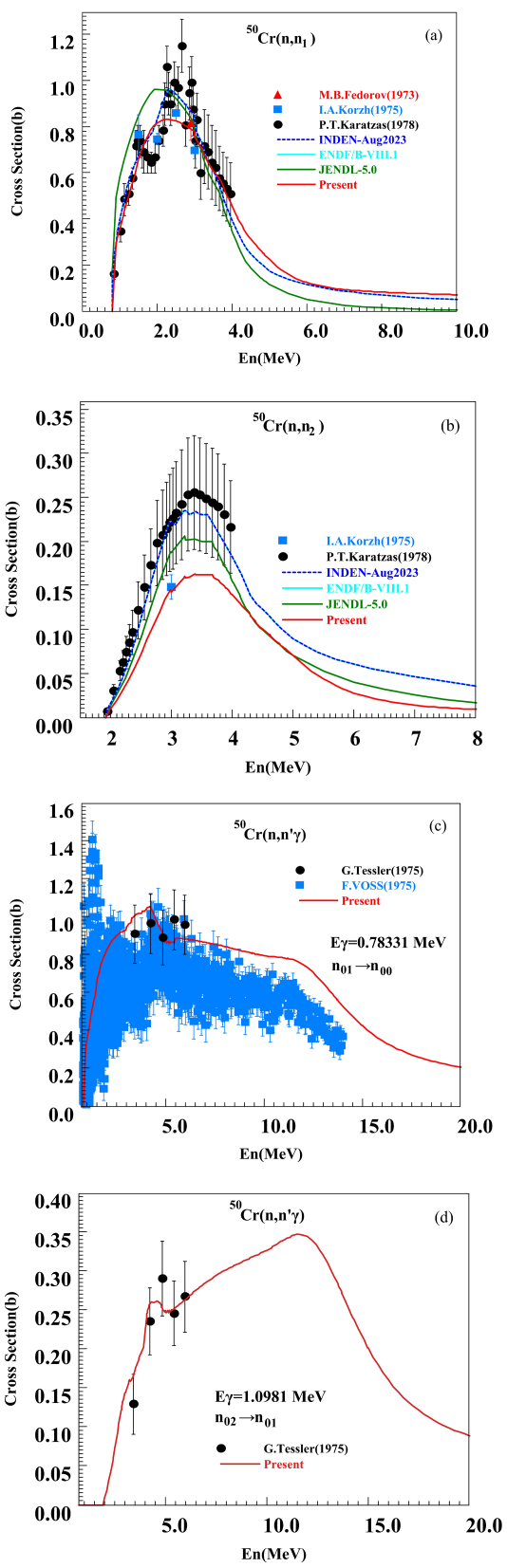

Fig. 16. (color online) Comparison of discrete levels' inelastic cross sections and inelastic scattering gamma production cross sections for ^{50}Cr between evaluated data (red curve) and experimental data (symbols).

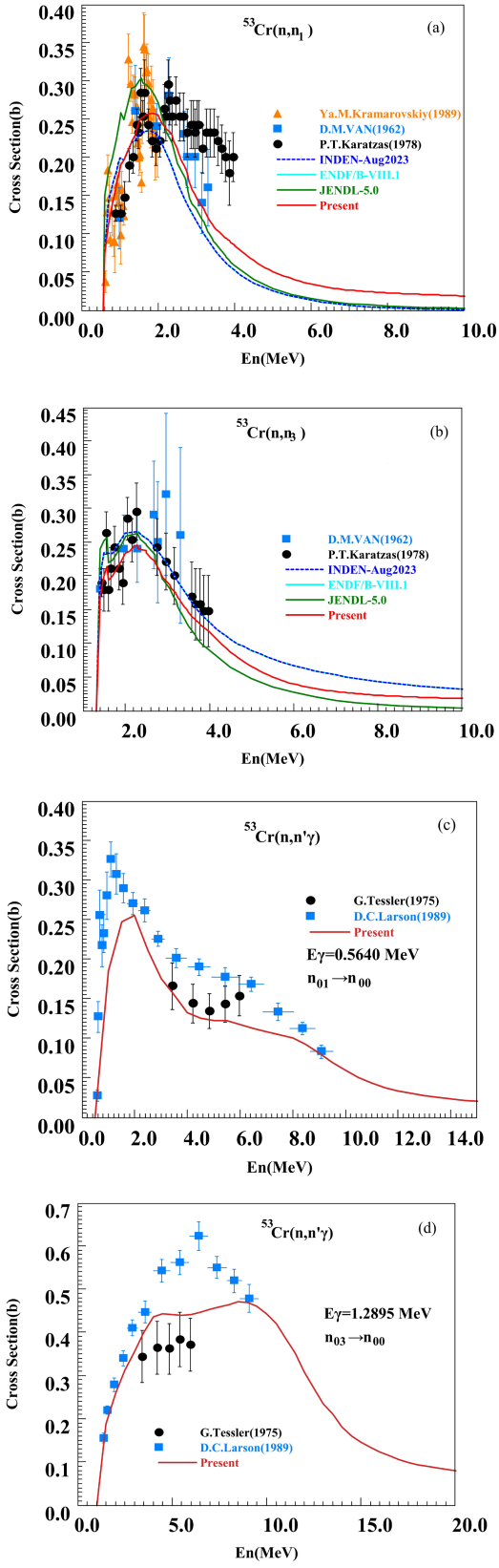

Fig. 17. (color online) Comparison of discrete levels' inelastic cross sections and inelastic scattering gamma production cross sections for ^{53}Cr between evaluated data (red curve) and experimental data (symbols).

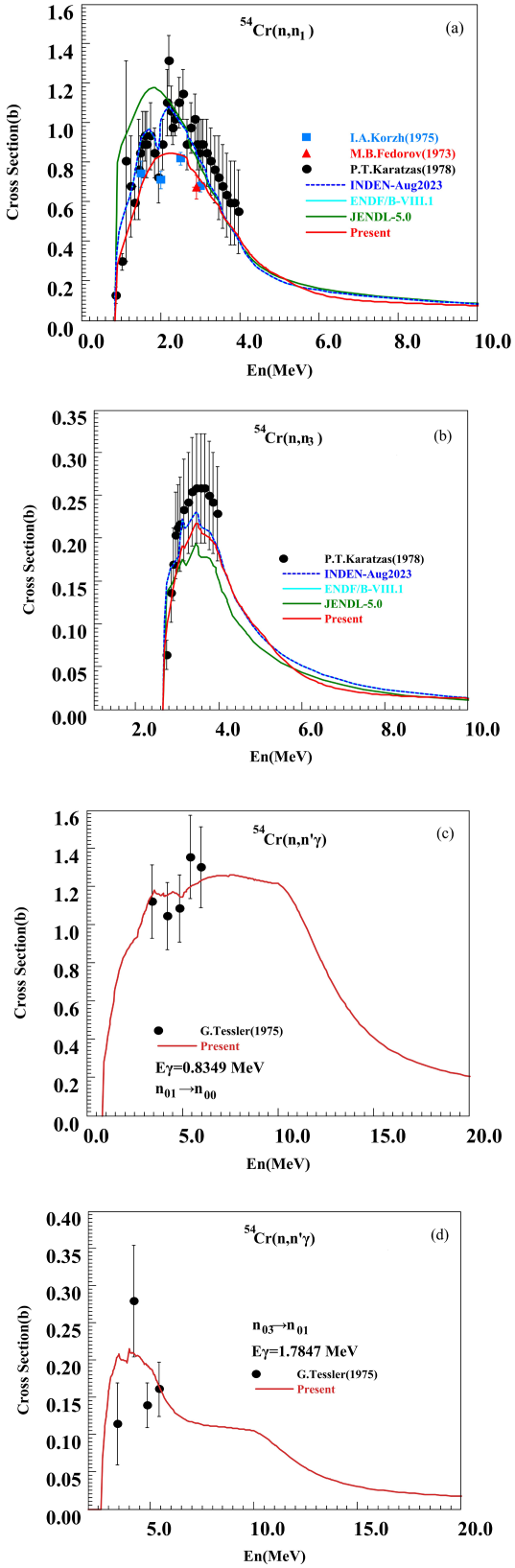

Fig. 18. (color online) Comparison of discrete levels' inelastic cross sections and inelastic scattering gamma production cross sections for ^{54}Cr between evaluated data (red curve) and experimental data (symbols).

Tessler et al. (1975) (EXFOR Entry: 10439) have measured the gamma-ray production cross sections for inelastic scattering on chromium isotope chains, and generally, the present results are reasonably consistent with those data.

The results of (n,γ) cross sections are compared with available experimental data as well as evaluated data from ENDF/B-VIII.1 and JENDL-5.0. Most experimental data are concentrated in the resonance energy region. The results for ^{50,52,53}Cr agree well with the existing experimental data, while there is a lack of experimental data for ^{54}Cr.

5. *The* (n,p) *reaction cross sections*

Fig. 19 shows the comparisons of evaluated results for the (n,p) reaction cross sections with the experimental data and the evaluated data. The results agree well with the existing experimental data. For ^{52}Cr, existing evaluated data show noticeable discrepancies above 20 MeV.

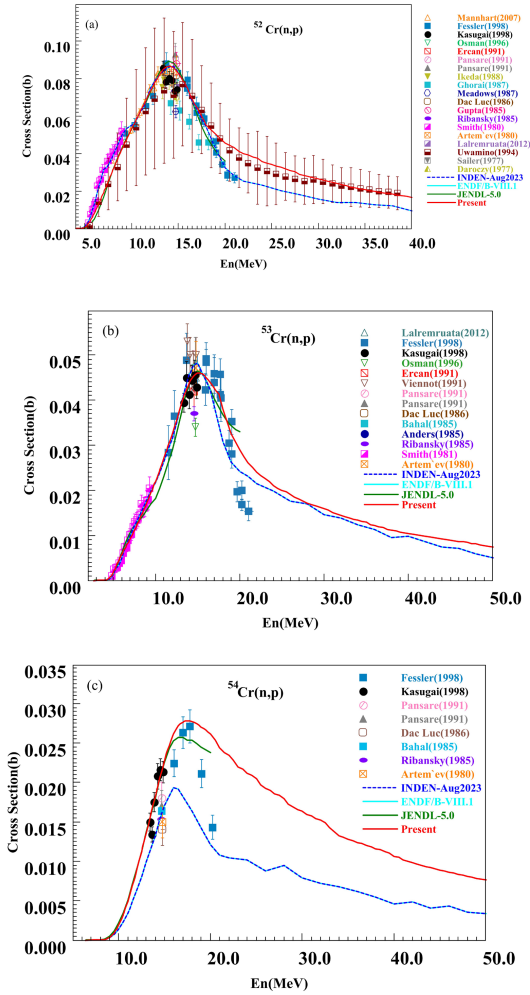

Fig. 19. (color online) Comparison of ^{52,53,54}Cr(n,p) cross sections between evaluated data (red curve) and experimental data (symbols).

Our results are in good agreement with the experimental data for natural Cr$(n,x)^{52}$V reported by Uwamino et al. within the energy range of 5.5–38.5 MeV. Analysis indicates that the natural Cr$(n,x)^{52}$V cross sections measured by Uwamino et al. (1994) mainly originate from the ^{52}Cr$(n,p)^{52}$V and ^{53}Cr$(n,x)^{52}$V reaction channels, while the ^{54}Cr$(n,t)^{52}$V cross sections is about 1 b and its contribution is negligible. In the following Section (8), Fig. 24(b) and Fig. 25 are shown that the weighted sum of the individual reaction cross sections agrees well with the experimental data for natural Cr, and each reaction channel is consistent with the corresponding experimental data, thus providing strong support for the validity of the ^{52}Cr$(n,p)^{52}$V cross sections presented in this work.

6. *The (n,α) and $(n,2n)$ reaction cross sections*

The comparison between the evaluated results and experimental data for the (n, α) reaction cross sections of ^{50,53,54,nat}Cr is shown in Fig. 20. The theoretical results for each isotope agree well with the experimental values, and their weighted sum is consistent with the experimental data for natural Cr. For the (n, α) reactions on ^{50,52,53}Cr, only the experimental data reported by T. Khromyleva et al. (2018) (EXFOR Entry: 41653) are available, covering energy ranges of 4.7–7.2 MeV, 6.8–7.2 MeV, and 4.5–7.15 MeV, respectively; the evaluated results match these data well. The remaining data points in Fig. 20(a) are from measurements of the ^{50}Cr$(n,x)^4He$ cross sections. Given that the threshold for the $(n,n\alpha)$ reaction is 21.0 MeV, it can be considered that below 15 MeV cross sections originate entirely from the ^{50}Cr(n,α) reaction. The results in this work are in good agreement with the experimental data from I. Matsuyama et al. (1994) (EXFOR Entry:22358).

For the $(n,2n)$ reaction cross sections, the comparison results with experimental data, for ^{50,52,nat}Cr are shown in Fig. 21. The theoretical results agree well with the existing experimental data except for the ^{50}Cr$(n,2n)$ reaction, where the evaluation results are higher than experimental data above 25 MeV. Discrepancies exist among the current evaluated data, and more experimental measurements are anticipated. For ^{52}Cr$(n,2n)$ cross sections, our results are consistent with the recommended experimental data. The (n,α) and $(n,2n)$ theoretical results for ^{50,52,53,54}Cr, summed by isotopic abundances, agree well with natural chromium experimental data, as shown in Fig. 20(d) and Fig. 21(c). The evaluated results can reflect the systematic differences among isotopes and are consistent with the experimental data.

7. *The (n,d) and (n,t) reaction cross sections*

The theoretical result for ^{50}Cr(n,d) reaction cross sections agrees well with the experimental data from S. M. Grimes et al. (EXFOR Entry: 10827) in 1979, as shown

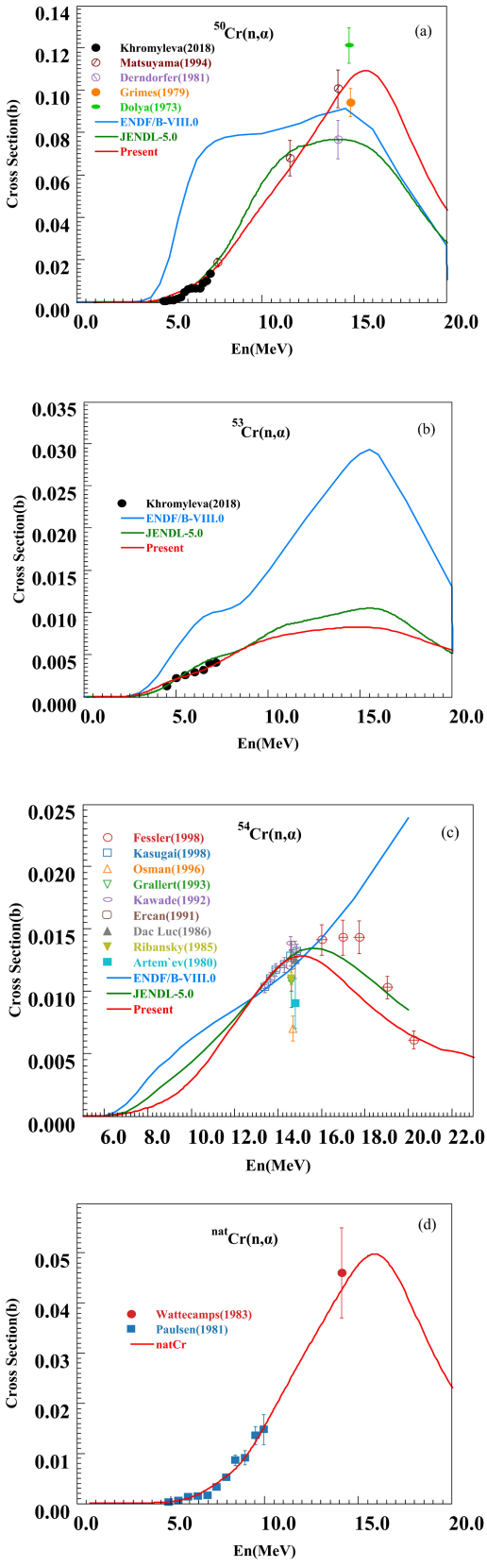

Fig. 20. (color online) Comparison of ^{50,53,54,nat}Cr(n,α) cross sections between evaluated data (red curve) and experimental data (symbols).

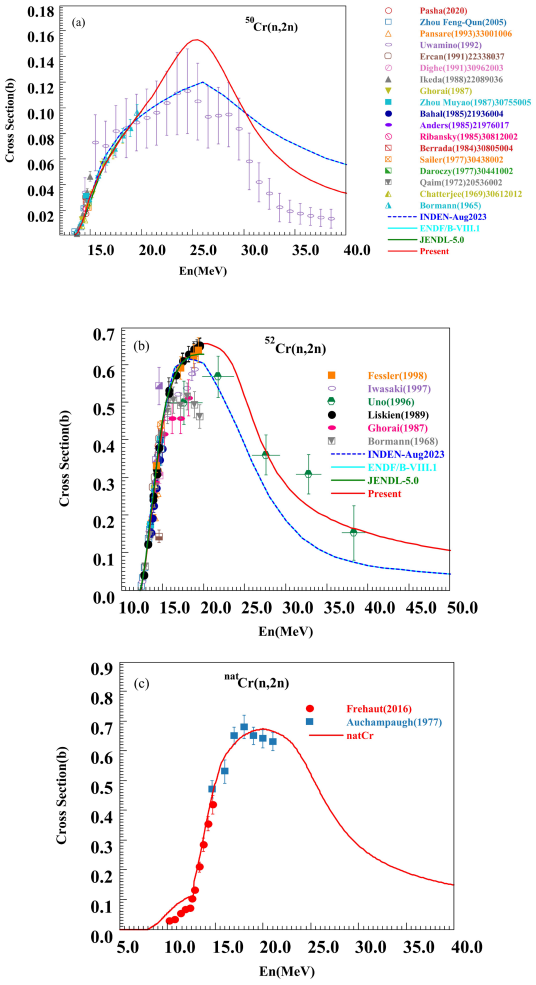

Fig. 21. (color online) Comparison of ^{50,52,nat}Cr$(n,2n)$ cross sections between evaluated data (red curve) and experimental data (symbols).

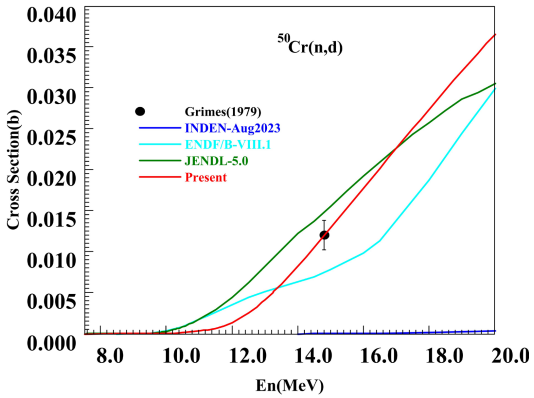

Fig. 22. (color online) Comparison of ^{50}Cr(n,d) cross sections between evaluated data (red curve) and experimental data (symbols).

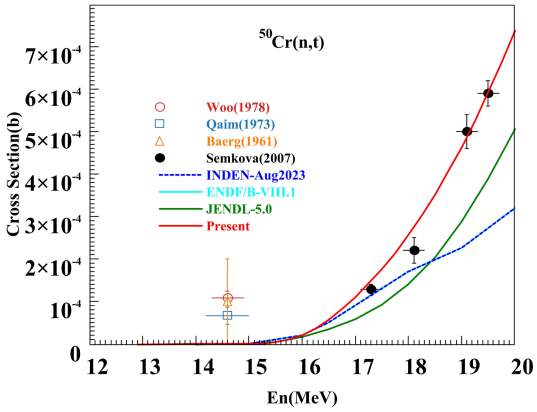

Fig. 23. (color online) Comparison of ^{50}Cr(n,t) cross sections between evaluated data (red curve) and experimental data (symbols).

in Fig. 22. The upper three sets of experimental data in Fig. 23 are ^{50}Cr(n,t) reaction cross sections, while the last set from V. Semkova et al.(2007) (EXFOR Entry: 22877) is the ^{50}Cr$(n,x)^{48}$V reaction cross sections. Below 20 MeV, the $(n,2np)$ reaction channel remains closed, and the cross sections contribution mainly come from the (n,t) reaction. The theoretical results agree well with the experimental data. Experimental data for the ^{52,53,54}Cr(n,t) reaction cross sections are lacking.

8. *The (n,x) reaction cross sections*

The experimental data retrieved from the EXFOR library for ^{50}Cr$(n,x)^{49}$V, ^{53}Cr$(n,x)^{52}$V and ^{54}Cr$(n,x)^{53}$V reaction cross sections include contributions from both (n,d) and (n,np) reactions. Therefore, the theoretical results for ^{50,53,54}Cr(n,d) and ^{50,53,54}Cr(n,np) reaction cross sections are summed and compared with the experimental data. The results are in excellent agreement with the $(n,x)^{49}$V, $(n,x)^{52}$V and $(n,x)^{53}$V data reported by Fessler et al. (EXFOR Entry: 22465, 22406), with discrepancies arising solely above 19 MeV where the evaluated results are slightly higher than the experimental measurements as shown in Fig. 24. After summing by isotopic abundances, the theoretical results for ^{52}Cr$(n,p)^{52}$V, ^{53}Cr$(n,np)^{52}$V + ^{53}Cr$(n,d)^{52}$V, and ^{54}Cr$(n,2np)^{52}$V+ ^{54}Cr$(n,t)^{52}$V reaction cross sections agree well with the experimental data for ^{nat}Cr$(n,x)^{52}$V reaction, as shown in Fig. 25.

At the same time, Fig. 26 shows the production cross sections of six types of fundamental particles (n, p, d, t, ^3He, and α) on ^{52}Cr below 200 MeV. Due to the lack of experimental data, the evaluation data relied on theoretical model calculations to give physically reasonable results.

B. Double differential cross sections

1. *Double differential cross sections for neutron emission*

Due to the lack of experimental data on the double

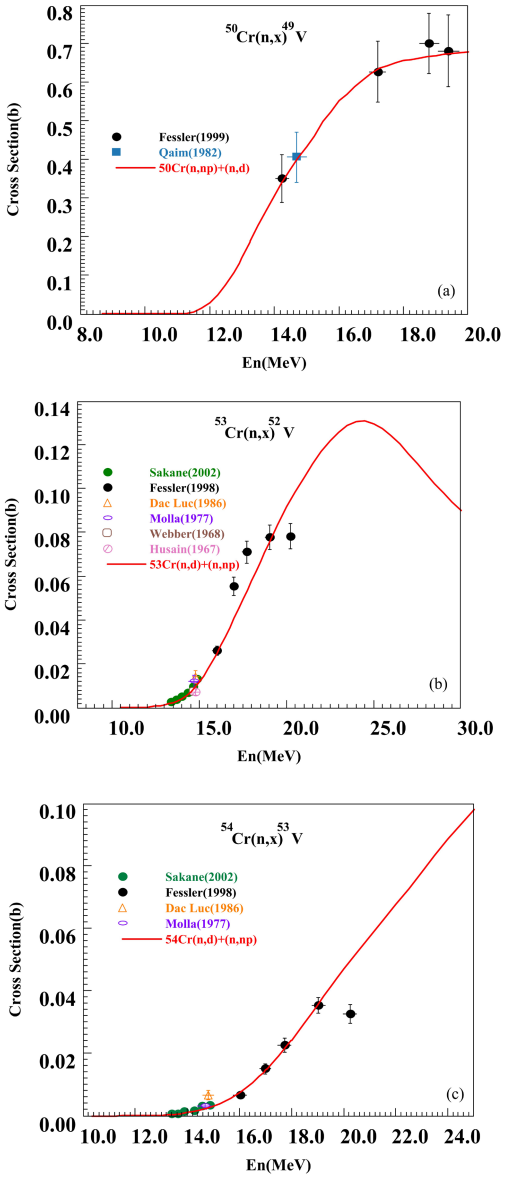

Fig. 24. (color online) Comparison of ^{50}Cr$(n,x)^{49}$V, ^{53}Cr$(n,x)^{52}$V and ^{54}Cr$(n,x)^{53}$V cross sections between evaluated data (red curve) and experimental data (symbols).

differential cross sections for neutron emission from ^{50,52,53,54}Cr(n,xn') reactions, the evaluated results of the double differential cross sections for neutron emission are compared and analyzed with the experimental data for natural chromium. S. Matsuyama et al. (1993) (EXFOR Entry: 22352) have published data on the double differential cross sections for neutron emission at an incident neutron energy of 14.1 MeV, with emission angles ranging from 20.0° to 150.0°. The consistency between the evaluated results for ^{50,52,54}Cr and the experimental data is depicted in Fig. 27. Evaluated results show good agreement with experimental data, reproducing both the elastic peak and intermediate-energy structures. For ^{50}Cr, the theoretical results fall below experimental data in the

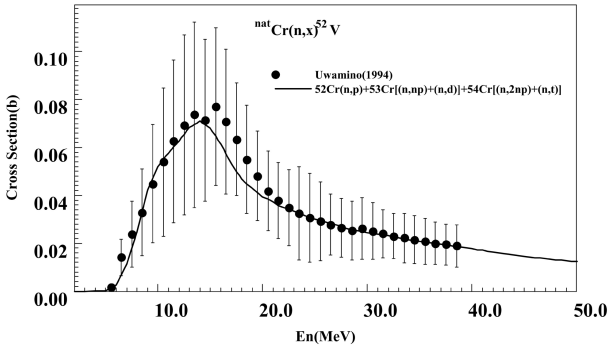

Fig. 25. Comparison of ^{nat}Cr$(n,x)^{52}$V cross sections between evaluated data (red curve) and experimental data (symbols).

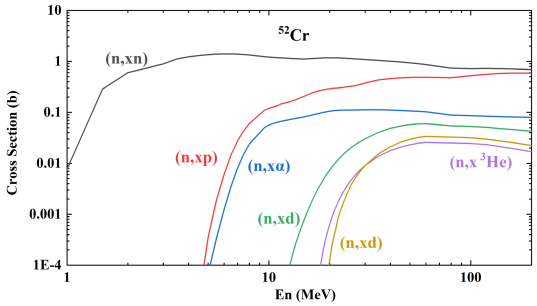

Fig. 26. (color online) The production cross sections of six fundamental particles (n, p, d, t, ^{3}He, and α) below 200 MeV.

low-energy region. We attribute this discrepancy to the ^{50}Cr$(n,2n)$ reaction threshold of 13.263 MeV: while evaluated results neglect contributions from secondary particle processes, experimental measurements may include such effects. As can be observed in Fig. 22(a), the ^{50}Cr$(n,2n)$ cross section at 14.1 MeV is significantly small.

D. Schmidt et al. (1997) (EXFOR Entry: 22411) provided experimental data on the double differential cross sections for neutron emission from ^{nat}Cr at incident neutron energies ranging from 7.95 to 14.10 MeV and emission angles between 25.0° and 160.0°.

The results are in good agreement with the experimental data across all angular positions within the full energy range. Given the substantial volume of experimental measurement data, we herein take 9 MeV, 10.79 MeV and 11.44 MeV as representative cases to illustrate the evaluated double differential cross sections for neutron emission from ^{52}Cr, ^{50}Cr, and ^{54}Cr in Fig. 28 to 30.

A. Takahashi et al.(1983) (EXFOR Entry: 21875) have measured the double differential cross sections for neutron emission at incident neutron energies ranging from 13.35 to 14.83 MeV, with emission angles between 18.0° and 159.0°. The comparison between the theoretical results for ^{50,54}Cr and the experimental data is shown in Fig. 31. The results basically give a satisfactory description of the experimental data in the whole emission energy range.

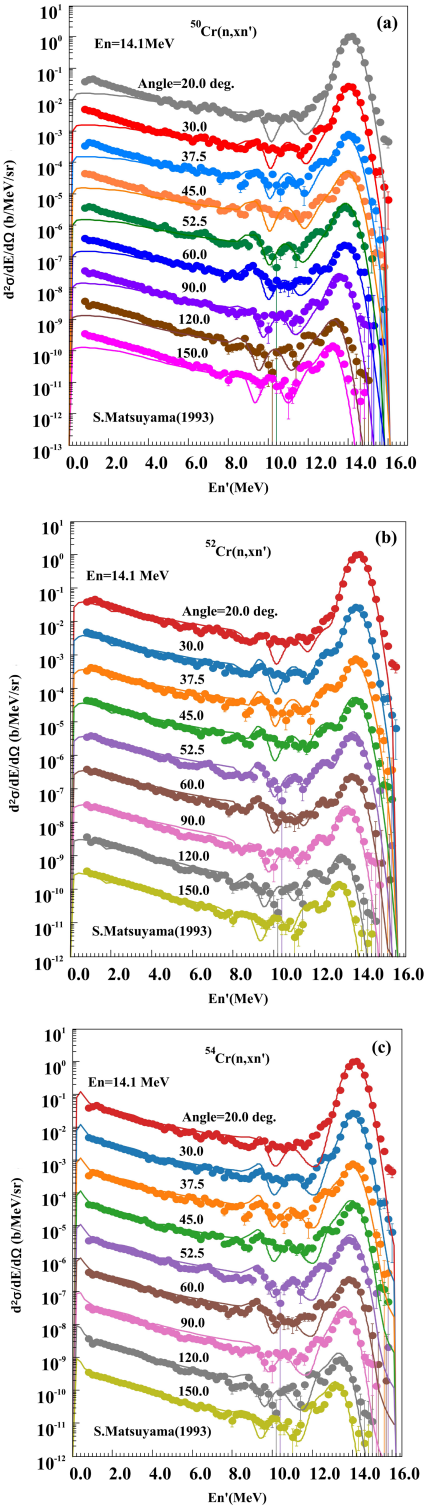

Fig. 27. (color online) Comparisons of ^{50,52,54}Cr(n,xn) double-differential cross sections at different angles for an incident energy of 14.1 MeV between the evaluated data (solid curves) and experimental data reported by S.Matsuyama (1993) (symbols). In each panel, the topmost curve for 20.0 degree remains the true reported values in the literature, and the other results from 30.0 to 150.0 degree are multiplied by factors of 0.1, 0.01, and so on, respectively.

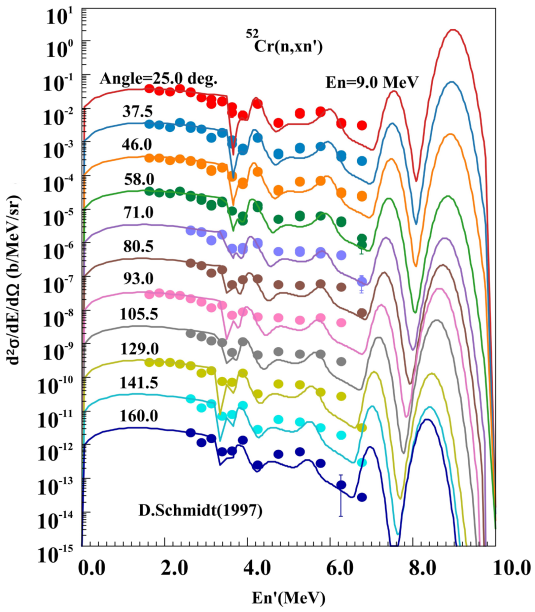

Fig. 28. (color online) Comparisons of ^{52}Cr(n,xn) double-differential cross sections at different angles for an incident energy of 9.0 MeV between the evaluated data (solid curves) and experimental data (symbols). The topmost curve for 25.0 degree remains the true reported values in the literature, and the other results from 37.5 to 160.0 degree are multiplied by factors of 0.1, 0.01, and so on, respectively.

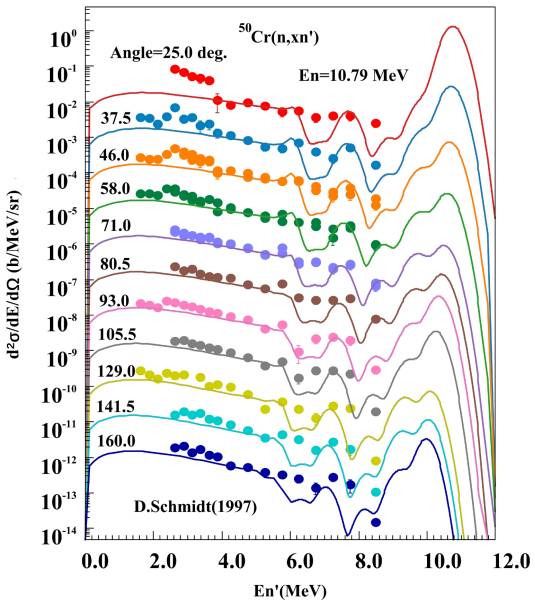

Fig. 29. (color online) Comparisons of ^{50}Cr(n,xn) double-differential cross sections at different angles for an incident energy of 10.79 MeV between the evaluated data (solid curves) and experimental data (symbols).The topmost curve for 25.0 degree remains the true reported values in the literature, and the other results from 37.5 to 160.0 degree are multiplied by factors of 0.1, 0.01, and so on, respectively.

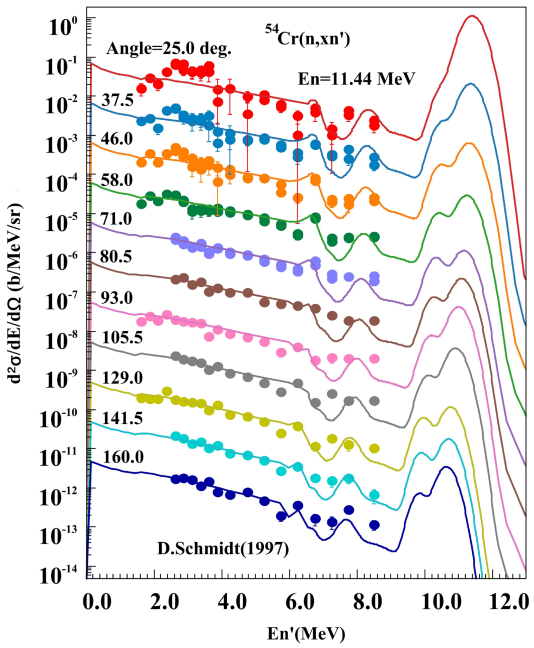

Fig. 30. (color online) Comparisons of ^{54}Cr(n,xn) double-differential cross sections at different angles for an incident energy of 11.44 MeV between the evaluated data (solid curves) and experimental data (symbols). The topmost curve for 25.0 degree remains the true reported values in the literature, and the other results from 37.5 to 160.0 degree are multiplied by factors of 0.1, 0.01, and so on, respectively.

The results and CENDL-3.2 evaluated data for ^{50,52,53,54}Cr, summed by isotopic abundances, are compared with natural chromium experimental data from A. Takahashi et al.(1983). The corresponding results are presented in Fig. 32. The present results can describe the structure of the discrete level contribution part more reasonably.

2. *Double differential cross sections for charged particle emission*

The double differential cross sections for the proton and alpha particle emissions are compared with the existing experimental data from ^{50,52}Cr in Fig. 33 to 34. The results basically agree well with the experimental data.

C. Energy spectra

1. *Energy spectra for charged particle emission*

No energy spectra experimental data are available for ^{53,54}Cr, while charged particle spectra experimental data exist for ^{50,52}Cr. Additionally, neutron emission energy spectra data have been measured for ^{52}Cr and natural chromium. From Fig. 35, the results basically give a satisfactory description of the experimental data for ^{50}Cr in the whole emission charged particle energy range. S. M.

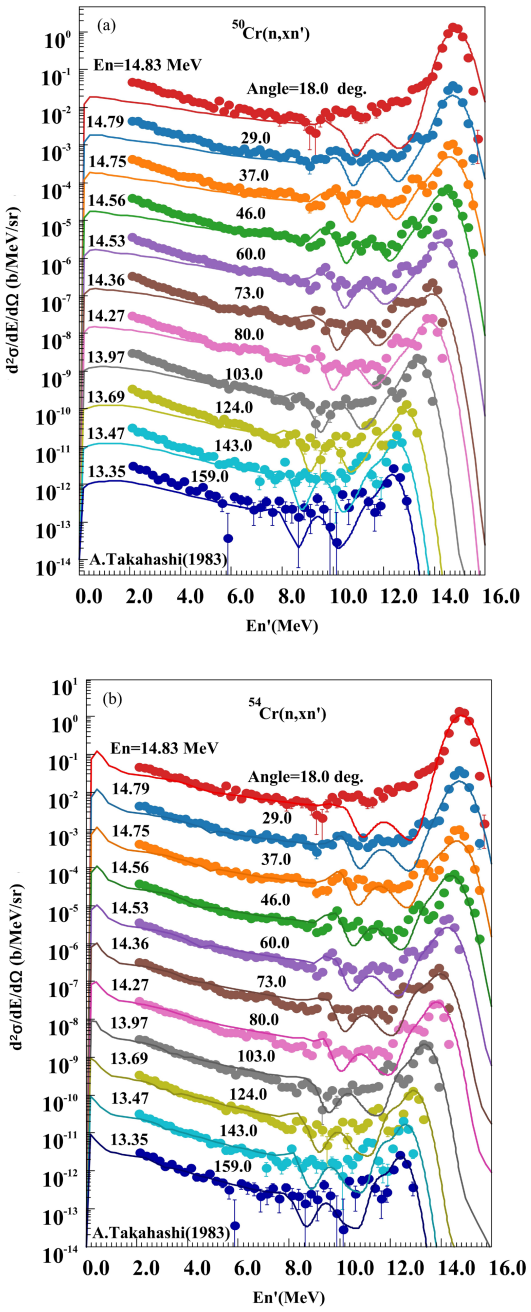

Fig. 31. (color online) Comparisons of ^{50,54}Cr(n,xn) double-differential cross sections at different angles for different incident energy from 14.83 MeV to 13.35 MeV between the evaluated data (solid curves) and experimental data reported by A.Takahashi (1983) (symbols). In each panel, the topmost curve for 14.83 MeV and 18.0 degree remains the true reported values in the literature, and the other results from top to bottom are multiplied by factors of 0.1, 0.01, and so on, respectively.

Grimes et al. (1979) (EXFOR Entry: 10827) have measured the energy spectra experimental data of proton, deuteron, and alpha particle emissions for ^{50}Cr and ^{52}Cr. One can find that generally, the present results are reasonably

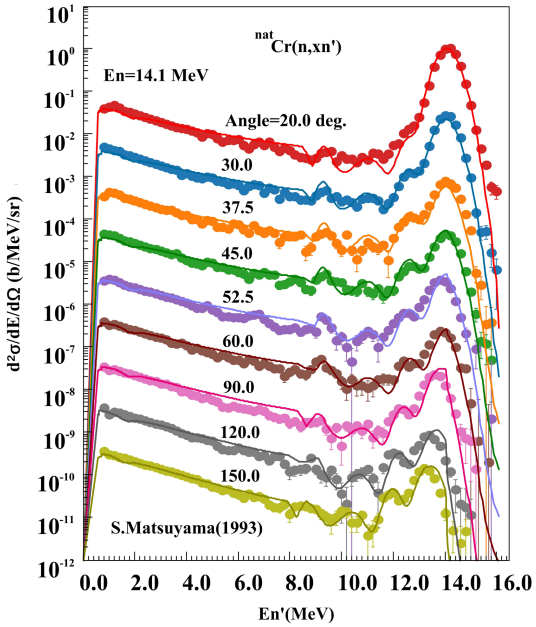

Fig. 32. (color online) Comparison of isotopically abundance-weighted (n,xn) double-differential cross sections for ^{50,52,53,54}Cr at different angles for an incident energy of 14.1 MeV between evaluated data (solid curves) and experimental data reported by S.Matsuyama (1993) (symbols). The topmost curve for 20.0 degree remains the true reported values in the literature, and the other results from 30.0 to 150.0 degree are multiplied by factors of 0.1, 0.01, and so on, respectively.

consistent with those data.

2. *Energy spectra for neutron emission*

The neutron emission energy spectra experimental data measured by D. Schmidt et al. (1997) (EXFOR Entry: 22411) of natural chromium is compared with theoretical results for ^{50,54}Cr as shown in Fig. 36. The results basically give a satisfactory description of the experimental data in the whole emission neutron energy range.

V. INTEGRAL TESTING

A. Criticality benchmark cases

Based on criticality benchmarks selected from the ICSBEP2006[27], 62 cases with sensitivity of $k_{\rm eff}$ to ^{52}Cr data exceeding 1% are identified. In these cases, ^{52}Cr primarily functions as a structural material. The selected experiments and their benchmark parameters are summarized in Appendix D.

The calculations are performed using the particle transport code MCNP, executed in parallel on the high-performance computing cluster of the China Nuclear Data Center (CNDC). All ACE-formatted files processed through NJOY2016[28]. Calculations based on the newly

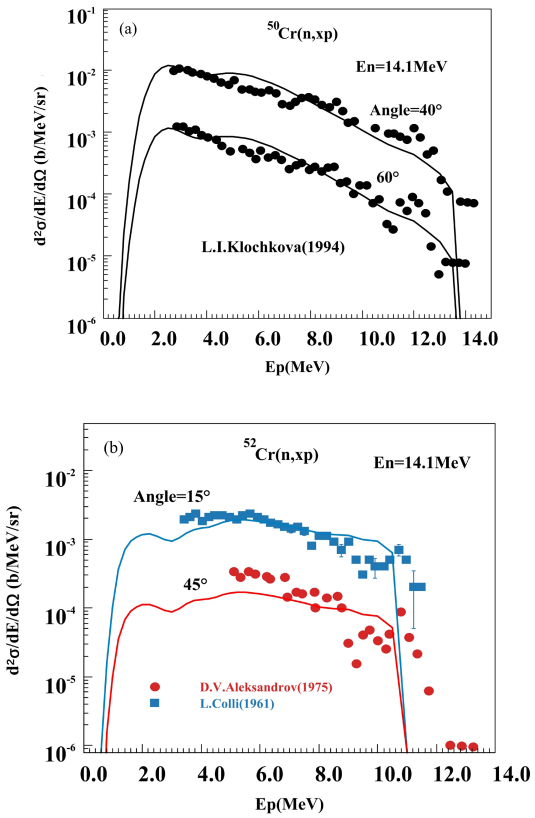

Fig. 33. (color online) Comparisons of ^{50,52}Cr(n,xp) double-differential cross sections at different angles for an incident energy of 14.1 MeV between the evaluated data (solid curves) and experimental data (symbols). In each panel, the top curve remains the true reported values in the literature, and the other results are multiplied by a factor of 0.1.

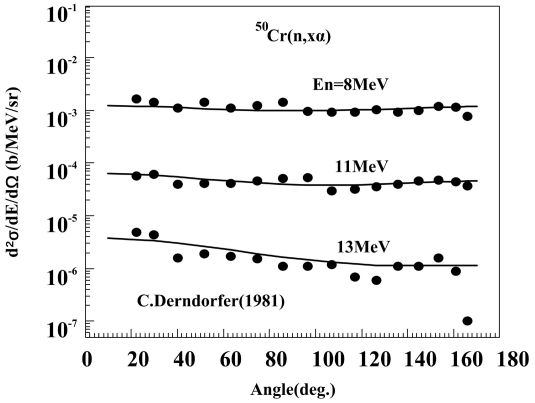

Fig. 34. Comparisons of double differential cross sections for alpha particle emission at incident energy of 8.0, 11.0 and 13.0 MeV between the evaluated data (solid curves) and experimental data reported by C.Derndorfer (1981) (symbols). In each panel, the topmost curve for 8.0 MeV remains the true reported values in the literature, and the other results from 11.0 MeV to 13.0 MeV are multiplied by factors of 0.1, 0.01 respectively.

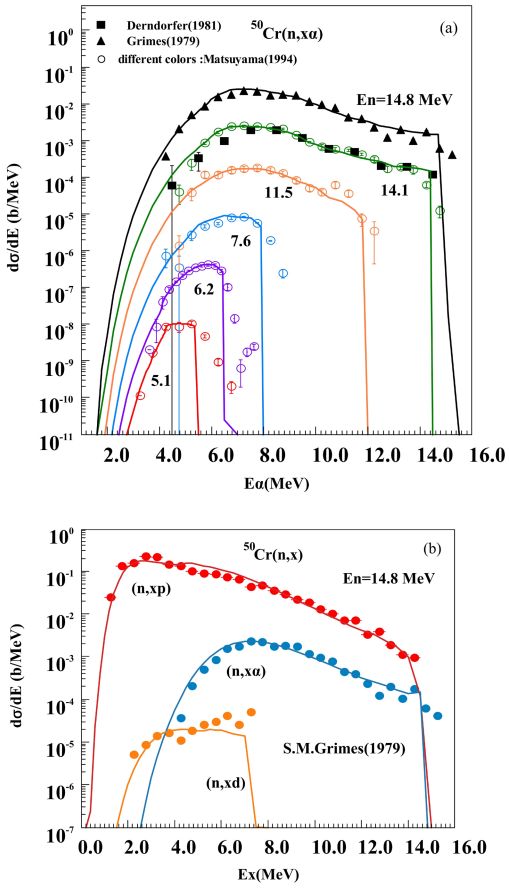

Fig. 35. (color online) Comparisons of the charged-particle emission energy spectra for ^{50}Cr between the evaluated data (solid curves) and the experimental data reported by D.Schmidt (1997) (symbols). In each panel, the topmost curve for 14.1 MeV remains the true reported values in the literature, and the other results from 12.7 MeV to 7.95 MeV are multiplied by factors of 0.1, 0.01, and so on, respectively.

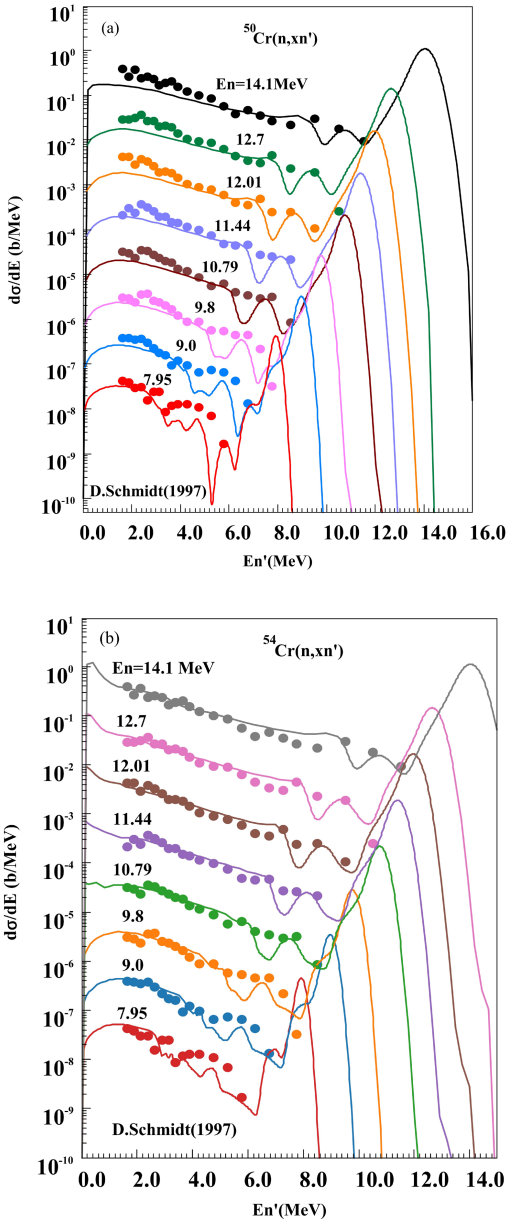

Fig. 36. (color online) Comparison of the neutron emission energy spectra for ^{50,54}Cr between the evaluated data (solid curves) and the experimental data reported by D.Schmidt (1997) (symbols). In each panel, the topmost curve for 14.1 MeV remains the true reported values in the literature, and the other results from 12.7 MeV to 7.95 MeV are multiplied by factors of 0.1, 0.01, and so on, respectively.

evaluated ^{52}Cr nuclear data are benchmarked against experimental reference values and compared with results obtained using CENDL-3.2, ENDF/B-VIII.1, JENDL-5.0, and JEFF-4.0. The computed-to-experimental (C/E) ratios for $k_{\rm eff}$ are presented in the Fig. 37 below.

Compared to CENDL-3.2, $k_{\rm eff}$ calculations for the intermediate-spectrum shielding facility using the newly evaluated ^{52}Cr nuclear data exhibit an overall reduction of ~100 pcm. For the PMI002_01 experiment specifically, the calculated $k_{\rm eff}$ shows a ~1000 pcm decrease relative to CENDL-3.2, demonstrating closer agreement with the benchmark value.

B. Shielding benchmark validation

The OKTAVIAN benchmark facility[29] is selected for shielding benchmark validation. Constructed at Osaka University, this facility comprises a high-current deuteron beam accelerator capable of generating pulsed D-T neutrons (10^3 neutrons/1.5 ns) or continuous D-T neutrons (3×10^{12} neutrons/s). Extensive fusion neutronics experiments have been conducted to investigate fundamental D-T fusion neutron transport characteristics. During 1984–1989, the Murata Laboratory at Osaka University employed the OKTAVIAN facility to measure neutron and gamma leakage spectra from spherical shell samples using the time-of-flight (TOF) technique, including a chromium sample sphere with a diameter of 40 cm.

Chromium in structural materials is modeled at natur-

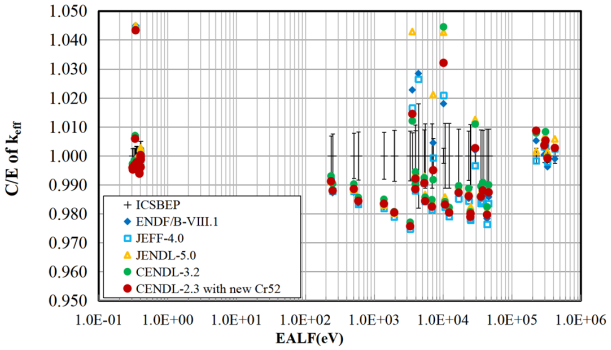

Fig. 37. (color online) The computed-to-experimental (C/E) ratios for Criticality Benchmark Validation of ^{52}Cr

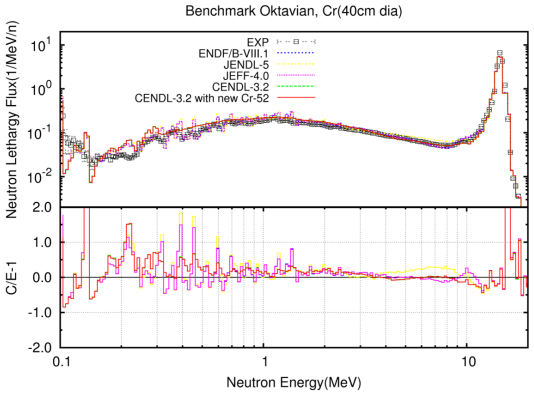

Fig. 38. (color online) Oktavian benchmark experiment validation results of ^{52}Cr (leaked neutron spectrum)

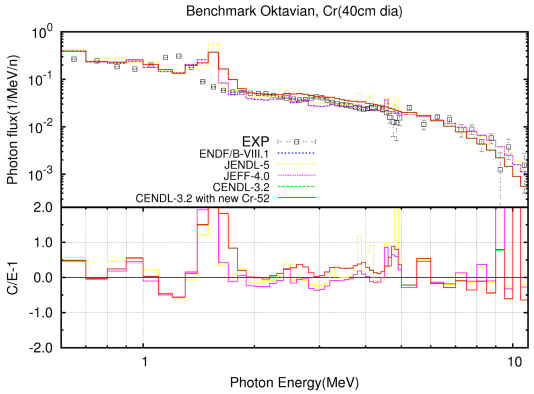

Fig. 39. (color online) Oktavian benchmark experiment validation results of ^{52}Cr (leakage photon spectrum)

al isotopic abundance. Evaluated nuclear data libraries employed include CENDL-3.2, ENDF/B-VIII.1, JENDL-5.0, and JEFF-4.0. The results of the OKTAVIAN benchmark experiment are shown in the Fig. 38 and 39. For the OKTAVIAN benchmark experiment, the calculated neutron leakage spectrum based on the newly evaluated ^{52}Cr nuclear data is on par with CENDL-3.2 and demonstrates satisfactory agreement with experimental measurements. The photon spectrum calculations for ^{52}Cr remain comparable to CENDL-3.2, though discrepancies are observed in the 1–2 MeV energy region, which require further investigation.

VI. CONCLUSIONS

In this work, we present a new evaluation and validation of neutron reaction data for ^{50,52,53,54}Cr isotopes at incident energies below 200 MeV, aiming to resolve discrepancies in reaction channels of existing libraries.

This study conducts a comprehensive assessment based on 571 sets of experimental data related to cross sections, angular distributions, energy spectra, and double differential cross sections. The experimental data evaluations are specially performed to improve the quality of the cross sections like (n,p), $(n,2n)$ et al, and the discrepancies are analyzed. At the same time, combining with the theoretical calculations via Chinese UNF and MEND, a complete set of neutron data for neutron energy below 200 MeV for chromium isotopes (^{50,52,53,54}Cr) are systematically obtained in this work. All the new results are compared with INDEN-Aug2023, ENDF/B-VIII.1, and JENDL-5. Better agreement with experimental data is observed in total, and the self-consistency of the evaluated results is also validated by reproducing the experimental element yields routed from various channels eg. the experimental ^{49}V production via ^{50}Cr(n,d) and ^{50}Cr(n,np).

All the data validated by involving 62 benchmark facilities from ICSBEP 2014, and the significant improvement is observed, especially for the PMI002_01 with Chromium isotopes as the major component, the calculated $k_{\rm eff}$ decreased by approximately 1000 pcm compared to CENDL-3.2, achieving better agreement with the benchmark value. Furthermore, the predicted neutron leakage spectrum in the OKTAVIAN shielding benchmark aligns well with experimental measurements.

Overall, the current evaluated data for ^{50}Cr, ^{52}Cr, ^{53}Cr, and ^{54}Cr exhibit high quality to support the future nuclear applications. In the energy region above 20 MeV, hundreds of nuclear reaction channels become accessible, resulting in strong competition among various pathways. This makes direct measurement of individual reaction cross sections extremely difficult. Therefore, for energies above 20 MeV, experimental measurements of energy spectra or double-differential cross sections of emitted particles—such as neutrons, protons, deuterons, tritons, helium-3, and alpha particles—are essential. These data will provide critical constraints for validating and refining theoretical models.

ACKNOWLEDGMENTS

The authors would like to thank Prof. Roberto Capote (IAEA) for the valuable information on Cr isotopes from the INDEN project and the insightful discussions.

APPENDIX A: ABBREVIATIONS AND ACRONYMS

APPENDIX B: THE LEVEL-DENSITY PARAMETER a AND THE PAIR CORRECTION PARAMETERS Δ

APPENDIX C: RECOMMENDED EXPERIMENTAL DATA

APPENDIX D: LIST OF CRITICALITY BENCHMARK EXPERIMENTS

Table A1. List of abbreviations and acronyms.

Abbreviation	Full Name	Abbreviation	Full Name
ACTIV	Activation	JENDL	Japanese Evaluated Nuclear Data Library
ADS	Accelerator-Driven Systems	JEFF	Joint Evaluated Fission and Fusion File
ATF	Accident-Tolerant Fuel	LONGC	Long counter
ASSOP	Associated particle	MOMIX	Mixed monitor
BF3	Boron Trifluoride detector	MAGSP	Magnetic spectrometer
BNL	Brookhaven National Laboratory	ORNL	Oak Ridge National Laboratory
BROND	Russian Nuclear Data Library	PHOTO	Photo-neutron
COINC	Coincidence	PROPC	Proportional counter
CHSEP	Chemical separation of products	PHD	Pulse-height discrimination
CENDL	Chinese Evaluated Nuclear Data Library	PSD	Pulse-shape discrimination
CSICR	Cesium-Iodide crystal	SIBAR	Silicon surface barrier detector
EC-JRC	European Commission Joint Research Centre	SOLST	Solid-state detector
EVAP	Evaporation neutrons	SILI	Silicon detector
EDE	Particle identification by 'E/Delta E' measurement	SCIN	Scintillation detector
ENDF/B	Evaluated Nuclear Data File/B	STANK	Standard tank (or neutron standard setup)
FISCH	Fission chamber	STTA	Stacked target irradiation
GELI	Germanium Lithium-drifted detector	SLODT	Slowing-down time
GE-IN	Germanium intrinsic detector	TOF	Time-of-flight
GSPEC	Gamma ray spectrometry	TENDL	TALYS-Based Evaluated Nuclear Data Library
HPGE	High-Purity Germanium detector	TRN	Transmission
IOCH	Ionization chamber	TELES	Counter telescope

Table B1. Level density and pair correction parameters of ^{50}Cr

Param.	Reaction Type										
	n,γ	n,n'	n,p	n,α	$n,^3\mathrm{He}$	n,d	n,t	$n,2n$	$n,n\alpha$	$n,2p$	$n,3n$
a	6.232	5.736	5.934	7.321	6.140	6.527	3.813	6.152	6.046	6.635	5.676
Δ	−2.5	0.041	−3.0	−0.23	0.2	−1.8	−0.06	−0.10	0.130	1.330	2.60

Table B2. Level density and pair correction parameters of ^{52}Cr

Param.	Reaction Type										
	n,γ	n,n'	n,p	n,α	$n,^3\mathrm{He}$	n,d	n,t	$n,2n$	$n,n\alpha$	$n,2p$	$n,3n$
a	6.080	5.416	5.7	6.235	5.868	6.255	7.034	6.232	6.140	6.524	5.736
Δ	−3.20	0.100	−1.90	0.05	0.130	−0.8	−0.460	−2.80	2.890	1.530	2.560

Table B3. Level density and pair correction parameters of ^{53}Cr

Param.	Reaction Type										
	n,γ	n,n'	n,p	n,α	$n,^3$He	n,d	n,t	$n,2n$	$n,n\alpha$	$n,2p$	$n,3n$
a	6.376	6.080	6.663	3.668	6.524	6.926	4.255	5.416	6.635	6.537	6.232
Δ	−2.5	0.075	0.070	0.000	0.073	−0.260	0.320	0.400	0.001	0.680	0.006

Table B4. Level density and pair correction parameters of ^{54}Cr

Param.	Reaction Type										
	n,γ	n,n'	n,p	n,α	$n,^3$He	n,d	n,t	$n,2n$	$n,n\alpha$	$n,2p$	$n,3n$
a	7.357	6.076	5.800	6.004	6.537	7.243	6.526	6.080	5.868	7.596	5.416
Δ	−2.50	0.100	−3.00	0.023	0.120	−0.650	−0.260	−0.590	2.730	1.330	2.400

Table C1. Recommended cross section experimental data of ^{50}Cr

Reaction	Year	First Author	Institute	Source	Method	Detector	En (MeV)	Points
(n,tot)	1972	A.I. Dyumin	Fiz.-Tekhnicheskiy Inst. Ioffe, Russia	−	COINC	SCIN	14.2	1
(n,el)	1977	I.A. Korzh	Inst. Yadernyh Doslidzhen, N.A. N.Ukraini, Kyiv, Ukraine		TOF	SCIN	1.5-3	4
(n,inl)	1962	D.M. Van Patter	Bartol Research Foundation, Swarthmore, PA, USA	P-^{7} Li	Ring Geometry	NAICR	0.98-3.31	10
(n,n')	1978	P.T. Karatzas	University of Massachusetts at Lowell, MA, United States of America	P-T	TOF	GELI, LONGC	0.84-3.97	73
	1975	I.A. Korzh	Inst. Yadernyh Doslidzhen, N.A. N.Ukraini, Kyiv, Ukraine	P-T	TOF	SCIN	1.5-3.0	5
	1973	M.B. Fedorov	Inst. Yadernyh Doslidzhen, N.A. N.Ukraini, Kyiv, Ukraine	D-D	TOF	SOLST	2.9	1
$(n,n'\gamma)$	1975	G. Tessler	Bettis Atomic Power Lab., Westinghouse, Pittsburgh, PA, USA	−	TOF	GELI, TELES	3.43-5.97	10
(n,γ)	1975	F. Voss	Karlsruhe Institute of Technology (KIT), Germany	EVAP	TOF	GELI, SCIN	0.799-14.0	1778
	2002	Yijun Xia	Sichuan Univ., Chengdu, China, People's Rep.	P-T; P-^{7} Li	−	HPGE	0.05-1.05	6
(n,p)	1994	L.I. Klochkova	Leningradskiy Tekhnologicheskiy Inst. Im. Lensoveta, Russia	D-T	EDE	TELES, PROPC, SCIN	14.1	1
(n,d)	1979	S.M. Grimes	Lawrence Livermore National Laboratory, Livermore, CA, USA	D-T	−	MAGSP, SIBAR	14.8	1
(n,t)	2007	V. Semkova	EC Joint Research Centre, Geel	D-T	ACTIV, GSPEC	HPGE, LONGC	17.3-20.6	5
(n,α)	2018	T. Khromyleva	Fiziko-Energeticheskii Inst., Obninsk, Russia	D-D	PHD	IOCH, FISCH	4.7-7.2	14
$(n,^4He)$	1994	I. Matsuyama	Tohoku Univ., Sendai, Japan	D-T, D-D, D-^{14} N, D-^{15} N	−	IOCH, TELES, SCIN	5.1-14.1	5
$(n,2n)$	2020	I. Pasha	Bangalore University, Bengaluru, India	D-T	ACTIV, STTA	HPGE	14.5	1
	2005	Zhou Feng-Qun	Lanzhou Univ., Lanzhou, China, People's Rep.	D-T	ACTIV	HPGE	13.5-14.6	4
	1987	S.K. Ghorai	Auburn University, Auburn, AL, USA	D-T	ACTIV, MOMIX, ASSOP	GELI	14.2-18.2	5
	1965	M.Bormann	Hamburg, Universitaet, Germany	D-T	ACTIV	−	13.6-19.6	9
$(n,3n)$	1992	Y.Uwamino	Univ. of Tokyo, Tokyo, Japan	P-^{9} Be	ACTIV	GE-IN	26.5-38.5	13

Continued on next page

Table C1-continued from previous page

Reaction	Year	First Author	Institute	Source	Method	Detector	En (MeV)	Points
$(n,x)^{49}$V	1999	A.Fessler	Forschungszentrum Juelich, Germany	D-D, D-T	ACTIV, GSPEC, STTA, CHSEP	HPGE,SILI	14.3-19.4	4
	1982	S.M.Qaim	Forschungszentrum Juelich, Germany	D-T	ACTIV	GELI	14.7	1

Table C2. Recommended cross section experimental data of ^{52}Cr

Reaction	Year	First Author	Institute	Source	Method	Detector	En (MeV)	Points
(n,tot)	2000	R.F.Carlton	Middle Tennessee State University, Murfreesboro, TN, USA	−	TOF,TRN	SCIN	0.00502-31.2	13620
	1972	A.I.Dyumin	Fiz.-Tekhnicheskiy Inst.Ioffe, St.Petersburg+Gatchina, Russia	D-T	COINC	SCIN	14.2	1
	1971	D.G.Foster Jr	Pacific Northwest Laboratories, Richland, WA,USA	D-LI	TOF	SCIN	2.34-14.9	240
(n,el)	1967	C.Thibault	CEA/Saclay, France	D-D	−	−	2.7	1
	1974	W.E.Kinney	Inst. Yadernyh Doslidzhen, N.A.N.Ukraini, Kyiv, Ukraine	D-D	TOF	SCIN	6.44-8.56	3
	1977	I.A.Korzh	Oak Ridge National Laboratory, Oak Ridge, TN, USA	P-T	TOF	SCIN	1.5-3.0	4
(n,inl)	2025	Tan Boyu	China Nuclear Data Center, China Institute of Atomic Energy	D-D	Prompt γ-ray measurement method	HPGE	5.62-7.95	3
	2007	L.C.Mihailescu	EC Joint Research Centre (EC-JRC), Geel	PHOTO	TOF	HPGE, FISCH	1.46-18.5	974
	1988	A.A.Lychagin	Fiziko-Energeticheskii Inst., Obninsk, Russia	D-T	TOF, COINC	SCIN	14.1	1
(n,n')	1962	D.M.Van Patter	Bartol Research Foundation, Swarthmore, PA, USA	P-^{7} Li	Ring Geometry	NAICR	0.98-3.31	10
	2007	L.C.Mihailescu	EC Joint Research Centre (EC-JRC), Geel	PHOTO	TOF	HPGE, FISCH	1.46-4.55	1088
	1998	D.Schmidt	Physikalisch-Technische Bundesanstalt, Braunschweig, Germany	D-D	TOF, PSD	SCIN	7.95-14.8	10
$(n,n'\gamma)$	1990	N.Olsson	Studsvik Science Research Laboratory, Nykoeping, Sweden	D-T	TOF	SCIN	21.6	1
	2025	Tan Boyu	China Nuclear Data Center, China Institute of Atomic Energy	D-D	Prompt γ−ray measurement method	HPGE	5.62-7.95	15
	2007	L.C.Mihailescu	EC Joint Research Centre (EC-JRC), Geel	PHOTO	TOF	HPGE, FISCH	1.46-18.5	4029
(n,γ)	1974	N.Frenes	Inst. fuer Isotopenforschung und Kernphysik, Vienna, Austria	D-T	PHD	GELI	14.1	1
(n,p)	2007	W.Mannhart	Physikalisch-Technische Bundesanstalt, Braunschweig, Germany	D-D	TOF, ACTIV, STTA	SCIN, HPGE, FISCH	7.86-14.5	15
	1998	A.Fessler	EC Joint Research Centre (EC-JRC), Geel	D-T, D-D	ACTIV, TOF, GSPEC	HPGE, BF_3, SCIN	9.31-21.1	22
	1991	A.Ercan	Cekmece Nucl. Res. Centre, Istanbul, Turkey	D-T	−	HPGE, BF_3	14.6	1
(n,d)	1979	S.M.Grimes	Lawrence Livermore National Laboratory, Livermore, CA, USA	D-T	−	MAGSP, SIBAR	14.8	1

Continued on next page

Table C2-continued from previous page

Reaction	Year	First Author	Institute	Source	Method	Detector	En (MeV)	Points
(n,α)	2018	T.Khromyleva	Fiziko-Energeticheskii Inst., Obninsk, Russia	D-D	PHD	IOCH, FISCH	4.7-7.2	14
$(n,2n)$	2020	I.Pasha	Bangalore University, Bengaluru, India	D-T	ACTIV	HPGE	14.5	1
	2007	W.Mannhart	Physikalisch-Technische Bundesanstalt, Braunschweig, Germany	D-D	TOF, ACTIV, STTA	SCIN, HPGE, FISCH	12.4-14.5	8
	2005	Zhou Feng-Qun	Lanzhou Univ., Lanzhou, China, People's Rep	D-T	ACTIV	HPGE	13.5-14.6	4
	1998	A.Fessler	EC Joint Research Centre (EC-JRC), Geel	D-T, D-D	ACTIV, TOF, GSPEC	HPGE, BF_3, SCIN	14.3-19.4	4
	1996	Y.Uno	Univ. of Tokyo, Tokyo, Japan	P-^{7} Li	ACTIV	GE-IN	17.6-38.3	5
	1989	H.Liskien	EC Joint Research Centre (EC-JRC), Geel	D-T	ACTIV	GE-IN, NAICR	12.7-19.5	24

Table C3. Recommended cross section experimental data of ^{53}Cr

Reaction	Year	First Author	Institute	Source	Method	Detector	En (MeV)	Points
(n,tot)	1972	A.I.Dyumin	Fiz.-Tekhnicheskiy Inst. Ioffe, St. Petersburg+Gatchina, Russia	D-T	COINC	SCIN	14.2	1
	1971	D.G.Foster Jr	Pacific Northwest Laboratories, Richland, WA, United States of America	D-LI	TOF	SCIN	2.26–14.8	248
(n,inl)	1962	D.M.Van Patter	Bartol Research Foundation, Swarthmore, PA, USA	P-^{7} Li	Ring Geometry	NAICR	0.98–3.31	10
(n,n')	1989	Ya.M.Kramarovskiy	Khlopin Radievij Inst., St. Petersburg, Russia	P-T	–	GELI, FISCH	0.63–1.98	40
	1978	P.T.Karatzas	University of Massachusetts at Lowell, MA, United States of America	P-T	TOF	GELI, LONGC	0.98–3.31	36
	1962	D.M.Van Patter	Bartol Research Foundation, Swarthmore, PA, United States of America	P-^{7} Li	Ring Geometry	NAICR	1.10–2.04	25
$(n,n'\gamma)$	1975	G.Tessler	Bettis Atomic Power Lab., Westinghouse, Pittsburgh, PA, USA	–	TOF	GELI, TELES	3.43–5.97	20
(n,γ)	1964	Fiz.Inst. Lebedev (FIAN), Moskva, Russia	Fiz.Inst. Lebedev (FIAN), Moskva, Russia	–	SLODT	SCIN, PROPC	2.9×10^{-5}–5.7×10^{-2}	35
(n,p)	2012	B.Lalremruata	Mizoram University, Aizawl, India	D-T	ACTIV	HPGE	14.8	1
	1998	A.Fessler	EC Joint Research Centre, Geel	D-T, D-D	ACTIV, TOF, GSPEC	HPGE, BF_3, SCIN	11.6–21.1	19
	1998	Y.Kasugai	Nagoya Univ., Nagoya, Japan	D-T	ACTIV	HPGE	13.4–14.9	6
	1981	D.L.Smith	Argonne National Laboratory, Argonne, IL, United States of America	D-D	ACTIV	GELI	4.82–9.34	23
(n,α)	2018	T.Khromyleva	Fiziko-Energeticheskii Inst., Obninsk, Russia	D-D	PHD	IOCH, FISCH	4.7–7.2	14
$(n,x)^{52}V$	2002	H.Sakane	Nagoya Univ., Nagoya, Japan	D-T	ACTIV, STTA	HPGE	13.4–14.9	6
	1998	A.Fessler	EC Joint Research Centre (EC-JRC), Geel	D-T, D-D	ACTIV, TOF, GSPEC	HPGE, BF_3, SCIN	16.0–20.2	5

Table C4. Recommended cross section experimental data of ^{54}Cr

Reaction	Year	First Author	Institute	Source	Method	Detector	En (MeV)	Points
(n,tot)	1972	A.I.Dyumin	Fiz.-Tekhnicheskiy Inst. Ioffe, St. Petersburg+Gatchina, Russia	D-T	COINC	SCIN	14.2	1
(n,el)	1977	I.A.Korzh	Inst. Yadernyh Doslidzhen, N.A.N. Ukraini, Kyiv, Ukraine	–	TOF	SCIN	1.5–3	4
(n,inl)	1962	D.M.Van Patter	Bartol Research Foundation, Swarthmore, PA, USA	P-^{7} Li	Ring Geometry	NAICR	0.98–3.31	10
(n,n')	1975	I.A.Korzh	Inst. Yadernyh Doslidzhen, N.A.N. Ukraini, Kyiv, Ukraine	P-T	TOF	SCIN	1.5–3.0	5
	1973	M.B.Fedorov	Inst. Yadernyh Doslidzhen, N.A.N. Ukraini, Kyiv, Ukraine	D-D	TOF	SOLST	2.9	1
$(n,n'\gamma)$	1975	G.Tessler	Bettis Atomic Power Lab., Westinghouse, Pittsburgh, PA, USA	–	TOF	GELI, TELES	3.43–5.97	9
(n,p)	1998	Y.Kasugai	Nagoya Univ., Nagoya, Japan	D-T	ACTIV	HPGE	13.4–14.9	6
	1998	Y.Kasugai	Nagoya Univ., Nagoya, Japan	D-T	ACTIV	HPGE	13.4–14.9	6
(n,α)	1998	Y.Kasugai	Nagoya Univ., Nagoya, Japan	D-T	ACTIV	HPGE	13.4–14.9	6
$(n,x)^{53}V$	2002	H.Sakane	Nagoya Univ., Nagoya, Japan	D-T	ACTIV, STTA	HPGE	13.4–14.9	6
	1998	A.Fessler	EC Joint Research Centre (EC-JRC), Geel	D-T, D-D	ACTIV, TOF, GSPEC	HPGE, BF_3, SCIN	16.0–20.2	5

Table C5. Recommended cross section experimental data of ^{nat}Cr

Reaction	Year	First Author	Institute	Source	Method	Detector	En (MeV)	Points
(n,tot)	2001	W.P.Abfalterer	Los Alamos National Laboratory, NM, USA	EVAP	TOF	SCIN	5.29–5.59	467
	1980	D.C.Larson	Oak Ridge National Laboratory, Oak Ridge, TN, USA	PHOTO	TOF	SCIN	2.0–80.6	685
(n,el)	1998	D.Schmidt	Physikalisch-Technische Bundesanstalt, Braunschweig, Germany	D-D	TOF, PSD	SCIN	7.95–14.8	10
	1987	N.Olsson	Studsvik Science Research Laboratory, Nykoeping, Sweden	D-T	TOF	SCIIN	2.16	1
(n,α)	1974	W.E.Kinney	Oak Ridge National Laboratory, Oak Ridge, TN, United States of America	D-D	TOF	SCIN	4.34–8.56	5
	1983	E.Wattecamps	EC Joint Research Centre, Geel	D-T	EDE, BCINT	PTOPC, SPLST	14.1	1
	1981	A.Paulsen	EC Joint Research Centre, Geel	D-D	EDE, BCINT	TELES, PROPC, SOLST	4.89–9.97	11
$(n,2n)$	2016	J.Frehaut	CEA/DAM Ile-de-France, Bruyeres-le-Chatel, Arpajon, France	D-D	–	STANK	10.2–14.8	11
	1977	G.F.Auchampaugh	Los Alamos National Laboratory, NM, USA	D-T	–	STANK, SCIN	14.7–21.0	7
$(n,x)^{52}V$	1994	Y.Uwamino	Univ. of Tokyo, Tokyo, Japan	P-^{9}Be	ACTIV	GE-IN	5.5–38.5	34

Table C6. Recommended angular distribution experimental data of ^{50,52,54,nat}Cr

Reaction	Year	First Author	Institute	Source	Method	Detector	En (MeV)	Points
^{50,54}Cr(n,el); ^{50,54}Cr(n,n')	1975	I.A.Korzh	Inst. Yadernyh Doslidzhen, N.A.N. Ukraini, Kyiv, Ukraine	P-T	TOF	SCIN	1.5–3.0	36
	1973	M.B.Fedorov	Inst. Yadernyh Doslidzhen, N.A.N. Ukraini, Kyiv, Ukraine	D-D	TOF	SOLST	2.9	7

Continued on next page

Table C6-continued from previous page

Reaction	Year	First Author	Institute	Source	Method	Detector	En (MeV)	Points
^{52}Cr(n,el); ^{52}Cr(n,n')	1982	I.A.Korzh	Inst. Yadernyh Doslidzhen, N.A.N. Ukraini, Kyiv, Ukraine	D-D	TOF	SCIN	5.0–6.0	29
	1974	W.E.Kinney	Oak Ridge National Laboratory, Oak Ridge, TN, USA	D-D	TOF	SCIN	6.44–8.56	54
^{nat}Cr(n,el)	1998	D.Schmidt	Physikalisch-Technische Bundesanstalt, Braunschweig, Germany	D-D	TOF, PSD	SCIN	7.95–14.8	376
	1997	A.B.Smith	Argonne National Laboratory, Argonne, IL, United States of America	D-D	TOF	SCIN	4.5–9.99	480

Table C7. Recommended double-differential cross sections experimental data of ^{50,52,nat}Cr

Reaction	Year	First Author	Institute	Source	Method	Detector	En (MeV)	Points
^{nat}Cr(n,xn)	1997	D.Schmidt	Physikalisch-Technische Bundesanstalt, Braunschweig, Germany	D-D	TOF, PSD	SCIN	7.95–14.1	4061
	1993	S.Matsuyama	Tohoku Univ., Sendai, Japan	D-T	TOF	SCIN	14.1	668
	1987	A.Takahashi	Osaka Univ., Osaka, Japan	D-T	TOF	SCIN	14.1	1094
	1983	A.Takahashi	Osaka Univ., Osaka, Japan	D-T	TOF	SCIN	13.4–14.8	677
^{50}Cr(n,x)^{1}H	1994	L.I.Klochkova	Leningradskiy Tekhnologicheskiy Inst. Im. Lensoveta, Russia	D-T	EDE	TELES, PROPC, SCIN	14.1	86
^{50}Cr(n,x)^{4}He	1981	C.Derndorfer	Inst. fuer Isotopenforschung und Kernphysik, Vienna, Austria	D-T	EDE	TELES, PROPC, CSICR	14.1	48
^{52}Cr(n,x)^{1}H	1975	D.V.Aleksandrov	Leningradskiy Tekhnologicheskiy Inst. Im. Lensoveta, Russia	–	Counter telescope method	TELES	14.1	29
	1961	L.Colli	Centro Informazioni Studi ed Esperienze (CISE), Milan, Italy	D-T	COINC	TELES, PROPC, SCIN, COIN, CSICR	14.1	35

Table C8. Recommended energy spectra experimental data of ^{50,52,nat}Cr

Reaction	Year	First Author	Institute	Source	Method	Detector	En(MeV)	Points
^{50}Cr(n,x)^{1}H	1994	L.I.Klochkova	Leningradskiy Tekhnologicheskiy Inst. Im. Lensoveta, Russia	D-T	EDE	TELES, PROPC, SCIN	14.1	46
^{50,52}Cr(n,x)^{1}H; ^{50,52}Cr(n,x)^{2}H; ^{50,52}Cr(n,x)^{4}He	1979	S.M.Grimes	Lawrence Livermore National Laboratory, Livermore, CA, USA	D-T	–	MAGSP, SIBAR	14.8	27
^{50}Cr(n,x)^{4}He	1994	I.Matsuyama	Tohoku Univ., Sendai, Japan	D-T, D-D, D-^{14}N, D-^{15}N	–	IOCH, TELES, SCIN	5.1–14.1	72
	1981	C.Derndorfer	Inst. fuer Isotopenforschung und Kernphysik, Vienna, Austria	D-T	EDE	TELES, PROPC, CSICR	14.1	11
natCr(n,xn)	1997	D.Schmidt	Physikalisch-Technische Bundesanstalt, Braunschweig, Germany	D-D	TOT, PSD	SCIN	7.95–14.1	149
	1993	S.Matsuyama	Tohoku Univ., Sendai, Japan	D-T	TOF	SCIN	14.1	74
	1987	A.Takahashi	Osaka Univ., Osaka, Japan	D-T	TOF	SCIN	14.1	72

Table D1. List of Criticality Benchmark Experiments for Macroscopic Examination of ^{52}Cr

No.	Identification	Benchmark k_{eff}	Uncertainty (1 sigma)	EALF (eV)
1	HEU-COMP-FAST-003-001	1.000	0.0085	23700.000
2	HEU-COMP-FAST-003-002	1.000	0.0088	37900.000
3	HEU-COMP-FAST-003-021	1.000	0.0092	43700.000
4	HEU-COMP-FAST-003-022	1.000	0.0090	35600.000
5	HEU-COMP-FAST-003-023	1.000	0.0093	46100.000
6	HEU-COMP-INTER-005-002	1.050	0.0080	3590.000
7	HEU-COMP-INTER-005-003	1.030	0.0060	7210.000
8	HEU-COMP-INTER-005-004	1.064	0.0180	4400.000
9	HEU-COMP-MIXED-002-003	1.000	0.0093	16900.000
10	HEU-COMP-MIXED-002-004	1.000	0.0087	3990.000
11	HEU-COMP-MIXED-002-005	1.000	0.0089	5360.000
12	HEU-COMP-MIXED-002-007	1.000	0.0086	3340.000
13	HEU-COMP-MIXED-002-008	1.000	0.0068	237.000
14	HEU-COMP-MIXED-002-009	1.000	0.0076	250.000
15	HEU-COMP-MIXED-002-010	1.000	0.0081	1390.000
16	HEU-COMP-MIXED-002-011	1.000	0.0088	1960.000
17	HEU-COMP-MIXED-002-012	1.000	0.0078	508.000
18	HEU-COMP-MIXED-002-013	1.000	0.0083	590.000
19	HEU-COMP-MIXED-002-014	1.000	0.0112	10700.000
20	HEU-COMP-MIXED-002-015	1.000	0.0111	6920.000
21	HEU-COMP-MIXED-002-016	1.000	0.0108	25000.000
22	HEU-COMP-MIXED-002-017	1.000	0.0112	12300.000
23	HEU-COMP-MIXED-002-018	1.000	0.0111	5510.000
24	HEU-COMP-MIXED-002-019	1.000	0.0107	3970.000
25	HEU-COMP-MIXED-002-020	1.000	0.0108	25200.000
26	HEU-MET-FAST-061-001	0.9998	0.0025	309000.000
27	HEU-MET-FAST-075-001	0.9985	0.0027	226000.000
28	HEU-MET-INTER-001-001	0.9966	0.0026	29400.000
29	HEU-SOL-THERM-038-001	1.000	0.0025	0.390
30	HEU-SOL-THERM-038-002	1.000	0.0025	0.310
31	HEU-SOL-THERM-038-003	1.000	0.0025	0.361
32	HEU-SOL-THERM-038-004	1.000	0.0025	0.389
33	HEU-SOL-THERM-038-005	1.000	0.0025	0.391
34	HEU-SOL-THERM-038-006	1.000	0.0025	0.313
35	HEU-SOL-THERM-038-007	1.000	0.0032	0.359
36	HEU-SOL-THERM-038-008	1.000	0.0026	0.355
37	HEU-SOL-THERM-038-009	1.000	0.0033	0.351
38	HEU-SOL-THERM-038-010	1.000	0.0026	0.370
39	HEU-SOL-THERM-038-011	1.000	0.0025	0.389
40	HEU-SOL-THERM-038-012	1.000	0.0025	0.388
41	HEU-SOL-THERM-038-013	1.000	0.0050	0.404

Continued on next page

Table D1-continued from previous page

No.	Identification	Benchmark k_{eff}	Uncertainty (1 sigma)	EALF (eV)
42	HEU-SOL-THERM-038-014	1.000	0.0050	0.406
43	HEU-SOL-THERM-038-015	1.000	0.0050	0.408
44	HEU-SOL-THERM-038-016	1.000	0.0050	0.409
45	HEU-SOL-THERM-038-017	1.000	0.0026	0.392
46	HEU-SOL-THERM-038-018	1.000	0.0032	0.385
47	HEU-SOL-THERM-038-019	1.000	0.0032	0.385
48	HEU-SOL-THERM-038-020	1.000	0.0032	0.385
49	HEU-SOL-THERM-038-021	1.000	0.0025	0.338
50	HEU-SOL-THERM-038-022	1.000	0.0027	0.330
51	HEU-SOL-THERM-038-023	1.000	0.0027	0.330
52	HEU-SOL-THERM-038-024	1.000	0.0026	0.407
53	HEU-SOL-THERM-038-025	1.000	0.0032	0.386
54	HEU-SOL-THERM-038-026	1.000	0.0032	0.385
55	HEU-SOL-THERM-038-027	1.000	0.0032	0.398
56	HEU-SOL-THERM-038-028	1.000	0.0025	0.371
57	HEU-SOL-THERM-038-029	1.000	0.0025	0.344
58	HEU-SOL-THERM-038-030	1.000	0.0027	0.338
59	MIX-MET-FAST-011-001	0.9897	0.0023	297000.000
60	MIX-MET-FAST-011-002	0.9998	0.0023	330000.000
61	PU-MET-FAST-033-001	0.9967	0.0026	422000.000
62	PU-MET-INTER-002-001	0.9869	0.0026	10200.000

References

[1] J. Bischoff, C. Delafoy, C. Vauglin, *et al*., Nucl. Eng. Technol. **50**, 223 (2018)

[2] H. Chen, X. M. Wang, R. Q. Zhang, Coatings **10**, 808 (2020)

[3] K.L. Murty, I. Charit, J. Nucl. Mater. **383**(1-2), 189 (2008)

[4] M. Fulger, K. Khumsa-Ang, M. Šípová, Ducu, *et al*., Coatings **13**(1), 58 (2023)

[5] H. R. Guo, Y. L. Han, T. Ye *et al*., Ann. Nucl. Energy **108**, 151 (2017)

[6] OECD Nuclear Energy Agency (NEA), *High Priority Request List (HPRL) for Nuclear Data*, (Paris: OECD NEA, 2022).

[7] G. P. A. Nobre, R. Capote, M. T. Pigni *et al.*, Nucl. Data Sheets (2025). Available as arXiv: 2511.03564.

[8] Joint Evaluated Fission and Fusion Project, *JEFF-4.0 Evaluated Data: neutron data [Data set]*. OECD Nuclear Energy Agency, https://databank.io.oecd-nea.org/data/jeff/40/, retrieved 18 March 2026.

[9] O. Iwamoto, N. Iwamoto, S. Kunieda, Nucl. Sci. Technol. **60**(1), 1 (2022)

[10] Z. G. Ge, R. R. Xu, H. C. Wu *et al*., EPJ Web Conf. **239**, 09001 (2020)

[11] A. I. Blokhin, E. V. Gai, A. V. Ignatyuk *et al*., Yad. Reak. Konst. **2**, 62 (2016)

[12] A. J. Koning, D. Rochman, J. -Ch. Sublet *et al*., Nucl. Data Sheets **155**, 1 (2019)

[13] D. Neudecker, B. Hejnal, F. Tovesson *et al*., EPJ Nucl. Sci. Technol. **4**, 21 (2018)

[14] A. M. Lewis, A. D. Carlson, D. L. Smith *et al*., EPJ Nucl. Sci. Technol. **9**, 34 (2023)

[15] A. M. Lewis, D. Neudecker, A. D. Carlson *et al*., EPJ Nucl. Sci. Technol. **9**, 33 (2023)

[16] J. S. Zhang, Nucl. Sci. Eng. **142**, 207 (2002)

[17] C. H. Cai, Nucl. Sci. Eng. **153**, 93 (2006)

[18] N. Otuka, E. Dupont, V. Semkova *et al*., Nucl. Data Sheets **120**, 272 (2014)

[19] A. Gandhi, A. Sharma, R. Pachuau *et al*., Chin. Phys. C **46**, 014002 (2022)

[20] A. Trkov, P. J. Griffin, S. P. Simakov *et al*., Nucl. Data Sheets **163**, 1 (2020)

[21] J. S. Zhang, Nucl. Sci. Eng. **114**, 55 (1993)

[22] G. X. Lu, L. Y. Dong, Z. F. Huang *et al*., Nucl. Phys. Rev. **16**, 246 (1999)

[23] P. D. Kunz, *Zero Range Distorted Wave Born Approximation*. (Colorado: University of Colorado, Department of Physics).

[24] R. Capote, M. Herman, P. Obložinský *et al*., Nucl. Data Sheets **110**, 3107 (2009)
[25] L. C. Leal, K. H. Guber, G. Arbanas *et al*., J. Korean Phys. Soc. **59**, 1644 (2011)
[26] B. Y. Tan, Z. H. Wang, H. Y. Wu *et al*., Acta Phys. Sin. **74**, 072901 (2025)
[27] OECD Nuclear Energy Agency, *International Handbook of Evaluated Criticality Safety Benchmark Experiments*. (Paris: OECD NEA, 2014).
[28] R. E. MacFarlane, D. W. Muir, R. M. Boicourt *et al.*, *The NJOY Nuclear Data Processing System*. (Los Alamos National Laboratory, 2016) LA-UR-17-20093.
[29] K. Sumita, A. Takahashi, T. Iida *et al*., Nucl. Sci. Eng. **106**, 249 (1990)